

Beryllium, Oxygen and Iron Abundances in Extremely Metal-Deficient Stars

Jeffrey A. Rich¹ & Ann Merchant Boesgaard¹

*Institute for Astronomy, University of Hawai'i at Manoa,
2680 Woodlawn Drive, Honolulu, HI 96822*

jrich@ifa.hawaii.edu

boes@ifa.hawaii.edu

ABSTRACT

The abundance of beryllium in the oldest, most metal-poor stars acts as a probe of early star formation and Galactic chemical evolution. We have analyzed high-resolution, high signal-to-noise Keck/HIRES spectra of 24 stars with $[\text{Fe}/\text{H}]$ from -2.3 to -3.5 in order to determine the history of Be abundance and explore the possibility of a Be plateau. We have determined stellar parameters of our sample spectroscopically, using equivalent widths of Fe I, Ti I and Ti II lines. We have determined O abundances from three OH features which occur in the same spectral region; this region is relatively uncrowded and has a well-determined continuum in these very/extremely metal-poor stars. We have supplemented this sample with reanalyzed spectra of 25 stars from previous observations so that our total sample ranges in $[\text{Fe}/\text{H}]$ from -0.5 to -3.5 . Our results indicate that the relationship between Be and $[\text{Fe}/\text{H}]$ continues to lower metallicities with a slope of 0.92 ± 0.04 . Although there is no indication of a plateau with constant Be abundance, the four lowest metallicity stars (below $[\text{Fe}/\text{H}]$ of -3.0) do show a Be enhancement relative to Fe at the 1σ level. A single relationship between Be and $[\text{O}/\text{H}]$ has a slope of 1.21 ± 0.08 , but there is also a good fit with two slopes: 1.59 above $[\text{O}/\text{H}] = -1.6$ and 0.74 for stars with $[\text{O}/\text{H}]$ below -1.6 . This change in slope could result from a change in the dominant production mechanism for Be. In the era of the formation of the more metal poor stars Be would be formed by acceleration of CNO atoms in the vicinity of SNII and in later times by high-energy cosmic rays bombarding CNO in the ambient interstellar gas. We find an excellent correlation between $[\text{Fe}/\text{H}]$ and $[\text{O}/\text{H}]$ and show that $[\text{O}/\text{Fe}]$ is near $+1.0$ at $[\text{Fe}/\text{H}] = -3.5$ declining to 0 at $[\text{Fe}/\text{H}] = 0$.

¹Visiting Astronomer, W. M. Keck Observatory jointly operated by the California Institute of Technology and the University of California.

Subject headings: stars: abundances; stars: evolution; stars: late-type; stars Population II; Galaxy: halo; Galaxy: disk

1. Introduction

The abundances of the rare light elements, Li, Be, and B, have revealed an amazing amount of information about an array of astrophysical issues. These include cosmology and nucleosynthesis in the Big Bang, Galactic chemical evolution, cosmic ray theory, and stellar interiors and stellar evolution. It is important to add more observations of Be to the large number of Li observations in order to make new progress in these research fields. Beryllium is the least complicated of the three light elements because it has only one known source of production and only one stable isotope, ^9Be . It is also less susceptible to depletion than Li in stellar interiors.

Observations of Primas et al. (2000a, 2000b) of Be in very metal poor stars led them to suggest the possibility of a Be plateau at very low $[\text{Fe}/\text{H}]$, possibly similar to the Spite lithium plateau (Spite & Spite 1982). The Li plateau in older stars is attributed to nucleosynthesis of Li during the Big Bang. If such a plateau exists, could it be similar to the Li plateau? Whereas the Li plateau is produced by nuclear reactions during the Big Bang, very little Be is produced in standard Big Bang nucleosynthesis (BBN): $N(\text{Be})/N(\text{H}) = 10^{-17}$ (Thomas et al. 1994). Models that include inhomogeneities in the early universe could produce a different mixture of light elements from the standard models (e.g. Malaney & Mathews 1992). Inhomogeneous models can create far more Be than standard models and the predictions of Orito et al. (1997) are 10^{-15} to 10^{-14} ; the implied plateau corresponds to 5×10^{-14} , which is tantalizingly close to the observed values.

Another possible cause of a Be “plateau” could be the creation of Be through spallation reactions in contained superbubbles created by multiple supernovae (Parizot 2000) or near hypernovae (Fields et al. 2002, Nakamura et al. 2006). Enrichment of the ISM in Be by such processes early in the history of the galaxy could result in a detectable plateau.

The lowest metal stars ($[\text{Fe}/\text{H}] < -3.0$) were formed early in the evolution of the Galaxy. By tracing the abundance of Be in these old stars, insight can be gained into the chemical history of the Galaxy. Beryllium is formed mainly through spallation reactions, which was proposed by Reeves, Fowler & Hoyle (1970) and further described by Meneguzzi, Audouze & Reeves (1971). The basic process is that high energy (~ 150 MeV) protons and neutrons bombard interstellar nuclei of C, N and O creating lighter isotopes. It has also been suggested that the “bullets” and the “targets” might be reversed near supernovae where C, N, and O

nuclei could be accelerated into the local interstellar gas including protons and neutrons (see, for example, Duncan et al. 1997, 1998, Lemoine, Vangioni-Flam & Cassé 1998).

Recent studies of Be in low metal stars include Boesgaard, Levesque & Rich (2008), Tan, Shi & Zhao (2009) and Smiljanic et al. (2009). All of these studies examine the Galactic evolution of Be through the relationships between the abundances of Be with Fe and Be with O and/or alpha-elements. The large study of Smiljanic et al. (2009) includes 90 stars and the determination of Be abundances of 73 halo and thick disk stars. They relied on Hipparcos parallaxes to find $\log g$, and adopted published values for temperature, $[\text{Fe}/\text{H}]$, $[\alpha/\text{Fe}]$, and microturbulent velocity. Their stars range in $[\text{Fe}/\text{H}]$ from -0.5 to -2.5 .

In this work we have obtained high signal-to-noise (S/N), high resolution spectra with the upgraded HIRES on the Keck I telescope of 24 stars covering values of $[\text{Fe}/\text{H}]$ of -2.32 to -3.45 to examine Be abundances at as low metallicities as possible. We supplement this sample with reanalyzed Keck/HIRES data from Boesgaard et al. (1999a) and Boesgaard (2007) and Subaru/HDS data from Boesgaard & Novicki (2006). Our total sample is 49 dwarfs and subgiants ranging in $[\text{Fe}/\text{H}]$ from -0.5 to -3.5 , with 34 stars below -2.0 . This is the most metal-poor set of stars which have been analyzed for Be abundances. Another difference from previous studies is that we have determined parameters spectroscopically.

2. Observations and Data Reduction

The Be II resonance lines, located in the UV spectral region at 3130.421 and 3131.065 Å, were used to determine the Be abundances. High S/N and high-resolution spectra are required to observe the Be doublet, which is weak in low metallicity stars. The upgraded High Resolution Echelle Spectrograph (HIRES) instrument on the Keck I telescope achieves the necessary requirements (Vogt et al. 1994). The spectral resolution for our setup was 48,000, and the light collecting area of the 10 m Keck telescope enables us to obtain S/N near 100 per pixel for our metal-poor sample. The pixel size on the upgraded CCD is 15μ . Such stars are uncommon and thus most are faint, especially in the UV wavelength region of the Be II lines. The observations reported here were carried out over 11 nights using the blue cross-disperser. The spectral range is approximately 3000 to 6000 Å. The new HIRES CCD is composed of three chips, one each for UV/blue (on which the Be doublet is located), green and red wavelengths. The quantum efficiency near 3100 Å is about 93%, making exposures of stars down to $V = 12$ possible.

Stars were selected based on their metallicity and observability. Stars with $[\text{Fe}/\text{H}]$ values of less than -2.4 dex were selected from a literature search. To obtain the best spectra, stars

were observed near the meridian, at the lowest possible airmass and atmospheric dispersion. Our aim was to observe stars with a declination range of $-20 < \delta < +60$; the latitude of Mauna Kea is $+19^{\text{deg}} 45'$. In order to obtain spectra of multiple objects with the required S/N, a cutoff at V of 12.5 was chosen. Table 1 shows observations of the stars analyzed with V magnitudes, literature values of $[\text{Fe}/\text{H}]$, the UT dates of the observations, the total exposure times and S/N per pixel near the Be doublet; in the cases where there are exposures on multiple nights the exposure times and S/N values are the totals. The median S/N = 104 and the mean is 106 per pixel.

HIRES data reduction was carried out using the IDL HIREMUX pipeline and standard IRAF routines. The pipeline was used to bias-subtract, flatten, extract and wavelength calibrate the spectrum from each individual exposure. IRAF was used to co-add multiple exposures of the same star and to fit continua to each combined, calibrated spectrum. G 64-37 was observed with HDS on Subaru, which has a similar but smaller wavelength range, with a maximum of $\sim 4500 \text{ \AA}$; see Boesgaard & Novicki (2006).

In addition to the new data obtained with the upgraded HIRES we have included data from Boesgaard et al. (1999a), as reanalyzed here, data from the Subaru 8 m telescope and HDS by Boesgaard & Novicki (2006) and data from Keck I with HIRES for three standard stars by Boesgaard (2007).

3. Data Analysis

The data were analyzed using IRAF and MOOG, a stellar synthesis and analysis program¹ (Snedden 1973). We used the 2002 version, which includes the UV opacity edges of the major atomic species. Equivalent widths of spectral lines were measured using IRAF routines. MOOG was used for two purposes: stellar parameter determination and abundance determinations. MOOG’s “abfind” driver was used with equivalent widths of Fe I, Fe II, Ti I, and Ti II lines to measure the metallicity, $[\text{Fe}/\text{H}]$, and determine T_{eff} and the surface gravity, $\log g$, of the stars in our sample. We used the “synth” driver to create synthetic spectra in order to measure Be and O abundances.

¹<http://verdi.as.utexas.edu/moog.html>

3.1. Stellar Parameters

Stellar parameters are needed to generate the stellar models used for spectral synthesis and abundance determination. We have chosen to determine our stellar parameters spectroscopically. We are dealing with spectral lines and need to know the temperature in the region of the atmosphere where the lines are formed. These temperatures seem more relevant for abundance work than the continuum-based color temperatures. It is generally the case that spectroscopic temperatures are lower than color temperatures because the continuum is formed deeper in the stellar atmosphere where the temperatures are higher.

Several Fe I and Fe II and Ti I and Ti II lines fall within the range of the HIRES CCD and can be used to determine $[\text{Fe}/\text{H}]$, T_{eff} and $\log g$, using an iterative method similar to that of Stephens (1999). Microturbulence, ξ , has a negligible effect on any of the measurements in this project, so a standard value of 1.5 km/s was used in all models (Magain 1984). We measured equivalent widths of 30-60 Fe I and 10 Fe II lines on the green and red chips of the HIRES CCD as well as 3 Fe I lines from the UV chip near the Be doublet. The Fe I lines covered a range in excitation potential from 0.86 to 3.98 eV and so could be used to derive the temperature. In addition we measured equivalent widths of 10-15 Ti I lines and 8-12 Ti II lines. A list of the lines measured, along with the excitation potential and the gf values, are given in Table 2. The values for gf come from the compilation presented in Stephens (1999) and Stephens & Boesgaard (2002) which gives the appropriate source references.

We have been careful to use only weak lines which would be on the linear portion of the curve of growth. This corresponds to $\log (W/\lambda) < -4.82$ which is ~ 75 mÅ at 5000 Å. For some stars we applied an even stricter limit of $\log (W/\lambda) < -5.15$ which is ~ 35 mÅ at 5000 Å. The measured equivalent widths are given in the tables in the Appendix. For two stars, G 64-12 and G 64-37, we adopted the parameters of Stephens & Boesgaard (2002) which were also determined spectroscopically; they used the same method as we did here, but they had a larger wavelength coverage toward the red and thus more useable lines.

Using an initial estimate for the stellar parameters and the measured equivalent widths, MOOG’s “abfind” driver was then used to calculate an Fe abundance for each line, as well as an average $[\text{Fe}/\text{H}]$ from the equivalent widths. MOOG also calculates the slope of each line’s calculated abundance versus its excitation potential (EP). If the temperature is correct, there should be no trend of abundance with EP.

Atomic abundances derived from two ions of the same species should give similar results. If the abundances do not agree, the value of $\log g$ can be adjusted and the abundances recalculated with MOOG. For the purposes of this project, MOOG was run iteratively by first calculating the abundance from Ti I lines using the temperature found via the Fe I lines,

then finding the abundance from Ti II and comparing the two sets of abundances. The value for $\log g$ is adjusted and the process can then be run iteratively between Fe I and Ti I plus Ti II abundances until $[\text{Fe}/\text{H}]$, T_{eff} and $\log g$ are calculated. (We have used the ionization balance between Ti I and Ti II, rather than Fe I and Fe II out of concern about NLTE effects on Fe I lines in metal-poor stars, e.g. Thévenin & Idiart 1999.) The stellar parameters used to calculate abundances are shown in the second, third and fourth columns of Table 3. Typical errors are $T_{\text{eff}} \pm 80$ K, $\log g \pm 0.2$ dex, $[\text{Fe}/\text{H}] \pm 0.15$ dex. Although our random errors on the temperatures determined spectroscopically are typically ± 80 K, we point out that there may be large (100-250 K) systematic differences in temperature determinations by other methods such as UBV and other photometric indices (and the potential uncertainties in the reddening corrections), the infrared flux method, Balmer-line profiles.

Although we have relied on the Magain (1984) value of 1.5 km s^{-1} for the microturbulence, we have checked the effect of using 1.0 km s^{-1} on the stellar parameters. On average with $\xi = 1.0 \text{ km s}^{-1}$, the value of T_{eff} is lower by 66 K, $\log g$ is lower by 0.15 and $[\text{Fe}/\text{H}]$ is lower by 0.03 dex. All of these are within the range of the uncertainties in our parameter determinations.

Ten of our stars have been observed for Li by Hosford et al. (2009). They use the excitation balance of Fe I to constrain their temperature scale and they constrain $\log g$ using theoretical isochrones. They present two sets of parameters for most of the stars appropriate for a main-sequence star and a subgiant-branch star. Our temperatures for the 10 stars in common are typically lower than theirs by -163 K on average. Our $\log g$ values are usually more in alignment with their subgiant branch gravities and on average are lower by -0.05 , well within the uncertainty of the determination. While the Li abundances are sensitive to temperature, but not to $\log g$, the Be abundances are quite insensitive to temperature, but are sensitive to $\log g$ (see §3.2 below.)

3.2. Abundance Determination and Errors

The difficulty in determining $A(\text{Be})$ in metal poor stars can be seen in Figure 1, which shows a comparison of a very metal poor star, BD +3 740 at $[\text{Fe}/\text{H}] = -2.95$ and one of much higher metallicity, HD 194598 at $[\text{Fe}/\text{H}] = -1.23$, from Boesgaard (2007). Both Be II lines are considerably weaker in the low metallicity star, BD + 3 740, and high signal-to-noise ratios are needed in spectra from such stars. The blending lines are also weaker, however, and the continuum placement is easier in the metal poor stars.

Once stellar parameters were calculated for each star, they were used to interpolate

models from the Kurucz (1993) grid. The models, coupled with a line list (adapted from Boesgaard et al. 1999a) generate a synthetic spectrum, which can then be compared to the data. The data are shifted in wavelength space to match the model and gaussian smoothing is applied to the model comparable to the shape of the line. Residuals of the synthetic spectrum versus the data can be viewed in MOOG in order to determine appropriate values for the wavelength shift and gaussian smoothing. The synthesis of the Be region of two stars is shown in Figure 2. Both Be and O abundances are optimized for the best fit in Figure 2.

The Be abundances determined this way are listed in Table 3 for each star.

Inasmuch as Li is more fragile with respect to nuclear destruction than Be, we looked at Li abundance determinations to ascertain whether there might be Be deficiencies. All of our stars except one (LP 752-17) have been observed for the abundance of Li, and all have normal Li-plateau abundances. Based on the criterion that normal Li-plateau values imply normal Be abundances, we conclude that none of these 23 stars has undergone Be depletion or dilution. Eleven of our stars appear in the Li compilation of Ryan et al. (1996) and nine are in the study of Ryan et al. (1999). The mean $A(\text{Li}) = 2.17 \pm 0.12$.

Although O is one of the most abundant elements in the universe, the determination of the O content in stars is not straight-forward. The three spectral features most commonly used are the OH lines in the UV, the O I triplet near 7774 Å and the [O I] line at 6300 Å. All three features present drawbacks, see e.g. Boesgaard (2001), Asplund & García Pérez (2001). In this work we are constrained to use the OH features in the UV which are near the Be II resonance lines. Our spectra do not extend past 6000 Å. Furthermore, the [O I] line is very weak in metal-poor stars, and in dwarfs and subdwarfs in particular; the O abundances found from [O I] for red giants may reflect altered O abundances due to nuclear processing of O along with mixing to the stellar surface.

There are electronic transition lines of OH that fall on the UV chip which we used to calculate the O abundance of each star using the “synth” driver as well. Some of these lines fall within the Be synthesis region, just redward of the Be line at 3130 Å; two others region are further toward the red at 3139 Å and 3140 Å. The line list for the 3139 region covers 1.5 Å and contains seven OH lines, the strongest of which is at 3139.17 Å with a $\log gf$ of -1.71 , as well as atomic lines. The line list in the 3140 region covers 1.1 Å and five OH transitions plus atomic lines. Generally, the O abundance agreed with the initial abundance calculated in the Be region. The average values are listed in Table 2, where the 3130 Å line has 2 times the weight of the other two lines. The synthesis fits for the two other OH line regions that we used are shown in Figure 3 for HD 140283 which has $[\text{Fe}/\text{H}] = -2.56$.

Errors in the abundance determinations are a result of error in the stellar parameters

as well as the accuracy of the synthesis fits. Errors in the abundances were determined by adjusting the stellar parameters $[\text{Fe}/\text{H}]$, T_{eff} and $\log g$ to see how it affected the abundance calculation. The largest effect on the Be abundances of any of the stellar parameters is due to uncertainties in $\log g$. For instance, a change in T_{eff} in ± 80 K results in a change in $A(\text{Be})$ of ± 0.02 and a change in $[\text{Fe}/\text{H}]$ of ± 0.2 dex results in a change in $A(\text{Be})$ of ± 0.01 . However, a change in $\log g$ of ± 0.2 results in a change of about ± 0.10 dex in $A(\text{Be})$. These errors are added in quadrature, which results in a typical error in $A(\text{Be})$ of about ± 0.12 dex. The individual errors are given in Table 3.

The errors on O abundances also result from the uncertainties in the stellar parameters and were determined in a similar manner. For the OH features, however, the error in T_{eff} has the largest effect on the determined abundance, followed by $\log g$. A change in T_{eff} of ± 80 K changes $[\text{O}/\text{H}]$ by ± 0.15 to 0.17 dex, while a change in $\log g$ of $+0.2$ only results in a change of $[\text{O}/\text{H}]$ by $+0.05$ to $+0.07$ dex. These uncertainties were added in quadrature and appear in Table 3.

Although the “missing” UV opacity has been blamed for inaccuracies in the Be abundances (Balachandran & Bell 1998), in these stars of such low metallicity, there is no problem of continuum placement and no issue of missing opacity. Similarly, the O abundances from the UV lines of OH are basically unaffected by opacity or continuum placement issues. We point out again that the 2002 version of MOOG includes the UV opacity edges of the dominant elements. In considering this issue Smiljanic et al. (2009) calculated the effect of an increase of 0.20 in $[\text{Fe}/\text{H}]$ (a factor of 1.6 as suggested by Balachandran & Bell 1998) on Be for a star with $[\text{Fe}/\text{H}] = -0.5$; they found that the difference in $A(\text{Be})$ was a negligible effect of only 0.022 dex.

Another source of uncertainty in the O abundances found from the OH features is in our use of standard LTE 1-D hydrostatic model atmospheres. Asplund & García Pérez (2001) use 3-D hydrodynamical model atmospheres to assess the effect of their more sophisticated models on the O abundance. They find that the corrections to $[\text{O}/\text{Fe}]$ increase with decreasing $[\text{Fe}/\text{H}]$ and also increase with decreasing gravity ranging from 0.3 to 0.4 dex at $[\text{Fe}/\text{H}] = -2.0$ to 0.5 to 0.6 dex at $[\text{Fe}/\text{H}] = -3.0$. They suggest that some of the calculated decrease in O may be mitigated by a full calculation of non-LTE effects.

We note that the absolute solar O abundance does not affect our $[\text{O}/\text{H}]$ values as the MOOG input value is just subtracted out. The same is true for the Be abundance; it does not matter whether we use the meteoritic Be abundance or some solar abundance.

3.3. New Be and O abundances from Previous Observations

We have reanalyzed the Keck/HIRES observations in Boesgaard et al. (1999a, 1999b) to use the newer version of MOOG from 2002. These observations were made with the original HIRES and due to the limited wavelength coverage of that CCD, we could not determine the stellar parameters spectroscopically. Instead we used the parameters from the 1999 papers with temperatures on the Carney (1983) scale. That temperature scale is consistent with the spectroscopic temperatures derived for the stars in this paper. For three stars we have lowered the temperature and achieve better fits. The new Be abundances were found by the same method used here - spectrum synthesis - and with the same line list. We have rederived the O abundances but use only three OH features (3130, 3139, and 3140 Å), as was done here for the newly observed stars. The new abundance results and the 1σ error estimates are presented here in Table 4 along with the stellar parameters and the 1σ errors on those.

The Be abundances do not differ much from those presented in Boesgaard et al. (1999a): on average they differ by -0.005 ± 0.077 with a range in $\Delta A(\text{Be})$ of -0.14 to $+0.15$ (in the sense of new minus old). The O abundances differ systematically when we use just the three clean OH features. The difference in $\Delta[\text{O}/\text{H}]$ ranges from -0.55 to $+0.12$ and the average is -0.22 ± 0.16 (again in the sense of new minus old). The differences result from our use of the three best OH features and ignoring the other weak and blended OH lines used in the earlier study.

3.4. Be and New O Abundances for Published Metal-Poor Stars

We have incorporated in this study the results on Be in metal-poor stars published by Boesgaard & Novicki (2006) (four stars), and the three Li-Be normal stars from Boesgaard (2007). These stars, their parameters and abundances are given in Table 4. We have determined O abundances in these stars in the same manner as above, from 3 OH features. Those results are presented in Table 5.

3.5. Be Abundance Comparisons

There are two stars in common in this study with Boesgaard et al. (1999a): BD +3° 740 and BD -13° 3442. For BD +3° 740 the parameters determined spectroscopically and photometrically agree well. The temperatures differ by -80 K, $\log g$ by 0.21, $[\text{Fe}/\text{H}]$ by -0.06 , $[\text{O}/\text{H}]$ by -0.10 , and $A(\text{Be})$ by -0.03 (in the sense of this study minus the reanalyzed

(Table 3) values from the data from Boesgaard et al. 1999a). In the case of BD -13° 3442 the spectroscopic gravity determined here is considerably higher (4.11 versus 3.50) and thus A(Be) is lower by 0.6 dex. The low value for $\log g$ from Boesgaard et al. (1999a) is very uncertain (± 0.44 in Table 3) so we adopt the results from this study. In addition, the S/N of the spectrum used here is 183 compared to the earlier one at 129.

There are two stars analyzed in this project that were previously considered by Primas et al. (2000a, 2000b), LP 815-43 and G 64-12. The values of A(Be) calculated from our data are slightly different from theirs: for LP 815-43 we derived A(Be)= -0.95 , while Primas et al. (2000a) found A(Be)= -1.09 and for G 64-12 we found A(Be)= -1.43 , whereas Primas et al. (2000b) derived A(Be)= -1.15 . Primas et al. (2000a, 2000b) adopted different stellar parameters for their stellar models, which would lead to different abundances. The parameters used in this project were determined spectroscopically and fit the data well. When the stellar parameters from Primas et al. (2000a) were applied to our data for LP 815-43, A(Be) was found to be about -1.10 , but other spectroscopic features in the Be region did not fit the data as well as with their parameters as with ours.

Although there are no stars from Smiljanic et al. (2009) in common with our new Keck data set in Table 3, there are 11 in common with our revised Boesgaard et al. (1999a) values in Table 4. Even though they used $\log g$ values derived from parallax and ours are from ionization balance, with the exception of one star (HD 219617) the agreement in $\log g$ is good with a mean difference of $+0.01 \pm 0.20$ (in the sense of this study minus Smiljanic et al.). The differences in A(Be) range from -0.17 to $+0.19$ dex (in the sense of this study minus Smiljanic et al.). The mean difference is $+0.02 \pm 0.13$ dex, indicating agreement within the individual errors. Two of the seven stars in Table 4 were also studied by Smiljanic et al. For HD 194598 our value for A(Be) is $+0.05$ dex higher and for HD 195633 our value is $+0.18$ dex higher.

There are four stars in common from Tables 4 and 5 with Tan et al. (2009): HD 76932, HD 132475, HD 140283, and HD 195633. The mean difference in our values minus theirs for A(Be) is -0.03 ± 0.16 dex with the largest difference (-0.24 dex) being that for HD 140283 caused by stellar parameter differences.

Interestingly, there are nine stars in common to the studies of Tan et al. (2009) and Smiljanic et al. (2009) from the same ESO/UVES data set. Their agreement for A(Be) is good with a mean difference (Smiljanic minus Tan) of $+0.07 \pm 0.09$ dex.

4. Results and Discussion

In this paper we discuss the abundance relationships between Be and Fe, between Be and O, and between Fe and O. We have acquired additional observations of Be in 34 more stars with $[\text{Fe}/\text{H}]$ between -0.7 and -2.5 . A paper by Boesgaard et al. (in preparation) will address the issue of the possibility of a spread in Be at a given $[\text{Fe}/\text{H}]$ and $[\text{O}/\text{H}]$ in the larger sample of 82 stars. That larger sample will also examine the potential connection between $A(\text{Be})$ and $[\text{O}/\text{Fe}]$ and the use of Be as a chronometer. Preliminary results from a smaller sample on these matters have appeared in a conference proceeding by Boesgaard et al. (2008).

4.1. Be and Fe Relationships

The Be abundances from Tables 3, 4, and 5 are shown in Figure 4 plotted against the values of $[\text{Fe}/\text{H}]$. The abundances show a trend of increasing $A(\text{Be})$ with increasing $[\text{Fe}/\text{H}]$.

The straight line between $A(\text{Be})$ and $[\text{Fe}/\text{H}]$ is

$$A(\text{Be}) = 0.92 (\pm 0.04)[\text{Fe}/\text{H}] + 1.41 (\pm 0.09).$$

One of our stars in Table 3, LP 831-70, has only an upper limit on $A(\text{Be})$; it is plotted as an inverted triangle in the figures and it has not been included in the linear fits. The slope of the least squares fit is 0.92 ± 0.04 . This slope is similar to that found by Boesgaard et al. (1999a) of 0.96 ± 0.04 . It is in agreement with the value of Molaro et al. (1997) of 1.07 ± 0.07 , but less steep than the recent values of 1.16 to 1.27 ± 0.07 found for the samples in Smiljanic et al. (2009). Tan et al. (2009) augmented their sample with the results for $A(\text{Be})$ and $[\text{Fe}/\text{H}]$ from Boesgaard et al. (1999a) in their Figure 7; considering their sample of 21 stars (omitting four “abnormal” Be values) they derive a slope of 1.10 ± 0.07 .

In Figure 5 we show two fits: one with a slope of 0.56 ± 0.07 for the stars with $[\text{Fe}/\text{H}] < -2.2$ and one of 1.07 ± 0.06 for stars with $[\text{Fe}/\text{H}] > -2.2$. The slope for the higher $[\text{Fe}/\text{H}]$ stars is in good agreement with those reported in the earlier studies, most of which contain only stars with $[\text{Fe}/\text{H}] > -2.5$. The shallower slope for the metal-poorest stars may indicate a slower, but gradual increase in Be as Fe increases in halo stars. On the other hand, the fit with one line is statistically no better or worse than the one with two lines. We have also tried making the break at $[\text{Fe}/\text{H}] = -2.7$; the fit is less good and the slopes are nearly the same at 0.57 ± 0.12 and 1.05 ± 0.05 . The two slopes intersect at -2.3 , not -2.7 .

The possible nucleosynthesis of Be in the Big Bang has been discussed by several authors (e.g. Boyd et al. 1989, Malaney and Fowler 1989, Alibes et al. 2002, Jedamzik and

Rehm 2006). Only in some inhomogeneous BB cosmologies is there enough Be produced to observe using current instruments. Our results do not seem to indicate a Be plateau at very low metallicities, as has been suggested by Primas et al. (2000a). Analyzing stars of even lower metallicities might provide further information, but observations become very time consuming, due to the faintness of the extremely low metal stars and the need for high S/N in order to observe the increasingly weak Be II lines. Our results in Figures 4 and 5 show no evidence for a plateau of constant $A(\text{Be})$, but a slower increase in Be with Fe at very low metallicities.

A more sensitive way to search for evidence of a plateau is to examine the Be abundance normalized to Fe, shown in Figure 6. The four stars with $[\text{Fe}/\text{H}] < -3.0$ do show enhanced Be relative to Fe. The best fit relationship is

$$[\text{Be}/\text{Fe}] = -0.08 (\pm 0.04) [\text{Fe}/\text{H}] - 0.01 (\pm 0.09).$$

The dashed line in the figure corresponds to the mean value of $[\text{Be}/\text{Fe}]$ for the 48 stars which is $+0.17 \pm 0.21$. This probable error bar is shown at the left in Figure 6 along the mean value line for $[\text{Be}/\text{Fe}]$. Although there is considerable scatter in $[\text{Be}/\text{Fe}]$ (the range is -0.21 to $+0.65$), the stars with the highest values of $[\text{Be}/\text{Fe}]$ are generally the lowest metallicity stars. But, as in Figures 4 and 5, there is not a plateau with a constant $A(\text{Be})$ or $[\text{Be}/\text{Fe}]$, but rather a smooth trend. The removal of the two Be-rich stars, HD 94028 and HD 132475 near $[\text{Fe}/\text{H}]$ of -1.5 , reduces the mean only to $+0.16$ but shows a clearer trend of high $[\text{Be}/\text{Fe}]$ at low $[\text{Fe}/\text{H}]$. (We note that Smiljanic et al. 2009 found a lower $\log g$ for HD 94028 and thus a lower Be abundance, putting it in alignment with the other stars.)

4.2. Be and O Relationships

The nucleosynthesis of Be is directly related to O as the spallation of abundant atoms like C, N, and O produce smaller atoms like Li, Be, and B. The spallation can occur 1) as high energy cosmic rays bombard CNO atoms in the ambient interstellar gas or 2) during supernovae explosions where atoms of CNO and protons are accelerated to high energies in the vicinity. These two mechanisms predict different relationships between Be and O.

In the more traditional GCR spallation the slope between $A(\text{Be})$ and $[\text{O}/\text{H}]$ would be 2 because the number of O atoms is proportional to the cumulative number of SN IIa (N) while the energetic protons are proportional to the instantaneous number of SN II (dN). The integral of NdN is kN^2 .

In the immediate vicinity of SN II the number of Be atoms would be proportional to

the number of O atoms; this would result in a slope of 1 between A(Be) and [O/H].

In Figure 7 we show the least-squares fit between A(Be) and [O/H]. The equation for the straight line is

$$A(\text{Be}) = 1.21 (\pm 0.08) + 1.32 (\pm 0.14).$$

There are reasons to suspect that Galactic evolution will play a role in the rate of the production of SN II. The early generations of stars will be massive stars which will produce supernova and begin to enrich the next generations of stars. These early SN will expel C and O which has been produced by nuclear fusion in their interiors prior to the supernova phase. The dominant mechanism creating Be atoms would thus be #2 above: acceleration of CNO from the SN explosion. Eventually, after multiple generations of stars have formed, the dominant mechanism would be #1 above: spallation by high energy cosmic rays in the interstellar gas.

In Figure 7 one can discern a possible change in slope so we have tried fitting two lines to the data. This result is shown in Figure 8. The oldest stars with the least O, $[O/H] < -1.4$, have a shallower slope of 0.74 ± 0.11 , while the stars with $[O/H] > -1.8$ have a steeper slope of 1.59 ± 0.15 . The transition occurs near $[O/H]$ of -1.6 .

For the stars with the lowest $[O/H]$ the relationship is

$$A(\text{Be}) = 0.74 (\pm 0.11) [O/H] + 0.40 (\pm 0.22).$$

For the stars with the higher values of $[O/H]$ the relationship is

$$A(\text{Be}) = 1.59 (\pm 0.15) [O/H] + 1.75 (\pm 0.20).$$

A changing slope is consistent with the change expected as the dominant production method for the spallation of Be changes. Other effects enter into the determination of the relationship between Be and O, such as mass outflow which may be lost during the process of star formation. Such effects would modify the predicted slopes of 1 and 2 to lower values. While we do not plan to discuss the models of Galactic chemical evolution, we point to these observations as a potential constraint on such models.

With respect to the $[O/H]$ abundances in Figures 7 and 8, we are concerned about the reduction in the O abundances through the use of 3-D hydrodynamic models as discussed by Asplund & García Pérez (2001). The decrease in O becomes larger as the metallicity decreases. The stars with the lowest values of A(Be) would have decreased $[O/H]$ values. The low Be points in those two figures would move to the left along the x-axis, thus favoring the 2-slope solution.

4.3. Fe and O Relationships

Our data enable us to reenter the controversy regarding the form of the relation between O and Fe. Our sample contains 49 stars which are all dwarfs and subgiants - no giants; the range in $\log g$ is 3.20 to 4.52. The temperatures range from turn-off stars at 6400 K to dwarf stars at 5500 K. Our star sample covers 3 orders of magnitude in $[\text{Fe}/\text{H}]$ from -0.5 to -3.5 with the bulk of the stars, 34, being below -2.0 and six of them ≤ -3.0 . This is a large uniform collection of similarly-analyzed stars which pushes the boundary to lower metallicities in an unevolved sample than was done, for example by Nissen et al. (2002), Fulbright & Johnson (2003), García Pérez et al. (2006). Although the Cayrel et al. (2004) study does go to low values of $[\text{Fe}/\text{H}]$, their stars are low-gravity evolved stars with $\log g$ ranging from 0.7 to 2.7; they find a mean $[\text{O}/\text{Fe}]$ of 0.7 with a dispersion of 0.17 dex and 0.47 after an uncertain correction for stellar surface inhomogeneities.

In Figure 9 we show the tight, linear relationship between $[\text{O}/\text{H}]$ and $[\text{Fe}/\text{H}]$ with a well-fitting slope of 0.70 ± 0.03 . The lowest metallicity stars merge well into the stars with higher values of $[\text{Fe}/\text{H}]$.

The relationship is

$$[\text{O}/\text{H}] = 0.692 (\pm 0.032) [\text{Fe}/\text{H}] - 0.076 (\pm 0.074)$$

Figure 10 shows the usual relationship where the element is normalized to Fe, in this case $[\text{O}/\text{Fe}]$. This can be fit well with a linear relationship where $[\text{O}/\text{Fe}]$ is ~ 1 at $[\text{Fe}/\text{H}] = -3.5$ and progresses towards 0 at $[\text{Fe}/\text{H}] = 0$. The equation is

$$[\text{O}/\text{Fe}] = -0.30 (\pm 0.03) [\text{Fe}/\text{H}] - 0.05 (\pm 0.07)$$

The continued upward trend toward lower metallicities in this relationship is similar to that found by Israelian et al. (1998, 2001), Boesgaard et al. (1999b), Nissen et al. (2002) although none of those studies went to as low values of $[\text{Fe}/\text{H}]$ as in this work. Fulbright & Johnson (2002) show a very similar trend with their ad hoc temperature which forces the parameters to yield agreement between the permitted and forbidden O features (see their Figure 13).

4.4. Implications

The linearity of the relation between $[\text{O}/\text{H}]$ and $[\text{Fe}/\text{H}]$ in Figure 9 is striking. And it implies that the 2 slope fit between $\text{A}(\text{Be})$ and $[\text{O}/\text{H}]$ (Figure 8) probably requires the 2 slope fit between $\text{A}(\text{Be})$ and $[\text{Fe}/\text{H}]$ (Figure 5). In turn this indicates that the upturn in

[Be/Fe] in Figure 6 at the lowest metallicities is significant. It is not evidence for a “plateau” in the Be abundance, but rather a change in the chemical history of the formation of Be. As discussed in §4.2 the spallation reactions occurring in the vicinity of SN II would dominate in the early episodes of Galactic evolution and there would be a flatter slope between Be and O. While still continuing to produce Be by this means, the standard GCR spallation would be more dominant in later eras, thus a steeper slope between Be and O. Again, we note that other stellar formation and evolution effects enter into the predicted relation and reduce both slopes.

5. Summary and Conclusion

We have used the upgraded HIRES on the Keck I 10m telescope to obtain high resolution, high signal-to-noise spectra of 24 very metal deficient stars from $[\text{Fe}/\text{H}] = -3.45$ to -2.32 . Of the 24 stars 19 have $[\text{Fe}/\text{H}] < -2.5$ and the other 5 are near -2.3 . (Even the large Be sample of Smiljanic et al. (2009) contains only three stars in our metallicity range, and those are at the high end of our range, with $[\text{Fe}/\text{H}] = -2.30, -2.35,$ and -2.48 and the latter has S/N of only 45.) Our data set was supplemented by spectra of 25 stars from Boesgaard et al. (1999a), Boesgaard & Novicki (2006) and Boesgaard (2007). For all these stars Be abundances determined from the Be II doublet at 3130 and 3131 Å and O abundances were found from 3 features of OH in the UV spectral region. For the newly observed stars stellar parameters were found spectroscopically using equivalent widths of Fe I for T_{eff} , and Ti I and Ti II for $\log g$. An iterative procedure was followed for the parameter determination and the Fe abundance. The stellar synthesis program MOOG was used in both *abfind* and *synth* modes to find the elemental abundances of Be, O, and Fe.

The full sample of 49 stars reveals a tight correlation between $[\text{O}/\text{H}]$ and $[\text{Fe}/\text{H}]$ with a slope of 0.69 ± 0.03 over 3 orders of magnitude in $[\text{Fe}/\text{H}]$ from -0.5 to -3.5 and over 2 orders of magnitude in $[\text{O}/\text{H}]$ from -0.4 to -2.5 . This is shown in Figure 9. One of the implications of this linear fit is that the stellar parameters and the abundance determinations give consistent results for the two sets of stars: the 24 very metal-poor stars (with spectroscopically determined parameters) and the reanalysis of the data from the three earlier papers (with photometrically-derived temperatures).

For one star we could only determine an upper limit on the Be abundance so our sample size is 48 for the Be data. Of the 48 stars 34 are below -2.0 in $[\text{Fe}/\text{H}]$ and five of those are ≤ -3.0 . This sample by far the largest sample of Be abundances found for low metallicity stars. In the sample of Smiljanic et al. (2009) of 73 Be detections, only four have $[\text{Fe}/\text{H}] < -2.0$ and four more at -2.0 .

We derive a linear relationship between $A(\text{Be})$ and $[\text{Fe}/\text{H}]$ which has a slope of 0.92 ± 0.04 and a linear relationship between $A(\text{Be})$ and $[\text{O}/\text{H}]$ with a slope of 1.21 ± 0.08 . Both plots can also be well fit by two linear relationships. The tightness of the relationship between the two abscissae, $[\text{Fe}/\text{H}]$ and $[\text{O}/\text{H}]$, lends support for the two-slope fits with $A(\text{Be})$. The slope change between $A(\text{Be})$ and $[\text{O}/\text{H}]$ from 0.74 ± 0.11 at low $[\text{O}/\text{H}]$ to 1.59 ± 0.15 occurs at $[\text{O}/\text{H}] = -1.6$. See Figure 8. The corresponding change point occurs at $[\text{Fe}/\text{H}] = -2.25$. See Figure 5. This “kink” occurs near -0.9 for $A(\text{Be})$.

The change in slope between $A(\text{Be})$ and $[\text{O}/\text{H}]$ would be a natural consequence of the change in the dominant mechanism of the formation of Be. In the early eras of the Galaxy, when massive stars become supernovae, the Be would be formed predominantly in the vicinity of the SN II where CNO atoms are accelerated to high energies and break up as they bombard protons, for example, and form lighter atoms such as Be. The slope would be a maximum of 1.0 as we find 0.74 for the stars with the lowest values of $[\text{O}/\text{H}]$. Later the spallation reactions could occur as high energy cosmic rays bombard CNO atoms in the interstellar gas. In that case the slope would be a maximum of 2.0, where we find 1.59. The change between the two mechanism’s dominance occurs as $[\text{O}/\text{H}]$ increases from -1.8 to -1.4 .

As we have found, the relationship between $[\text{O}/\text{H}]$ and $[\text{Fe}/\text{H}]$ is linear; the change in the slope between $A(\text{Be})$ and $[\text{Fe}/\text{H}]$ also results from the change in the dominant mechanism that forms Be. Whereas the formation of Be and O are related, the same cannot be said of Be and Fe. The Fe atoms are a product of stellar nucleosynthesis via the e-process and not directly connected to the formation of Be. The slope change is due to Be production, not Fe.

One of our goals was to search for a Be plateau at low metallicities, analogous to the Li plateau. We searched for this in our plot of $[\text{Be}/\text{Fe}]$ vs $[\text{Fe}/\text{H}]$ in Figure 6. We did not find evidence for a constant Be abundance at the lowest values of $[\text{Fe}/\text{H}]$, but rather an indication of a gradual increase in $[\text{Be}/\text{Fe}]$ toward the lowest $[\text{Fe}/\text{H}]$ values. As Figure 6 shows, the four stars with the lowest $[\text{Fe}/\text{H}]$ have enhanced $[\text{Be}/\text{Fe}]$ equivalent to the one sigma error. These data do not indicate that Be has been formed in an inhomogeneous-style Big Bang.

We have a large sample of low metal stars in which O and Fe abundances have been determined consistently so we can use the connection between $[\text{O}/\text{Fe}]$ and $[\text{Fe}/\text{H}]$ to learn about the early overproduction of O (formed in massive stars) relative to Fe (formed in intermediate-mass stars). We looked at the enhancement in $[\text{O}/\text{Fe}]$ as a function of $[\text{Fe}/\text{H}]$ in Figure 10. We find that the O enhancement decrease steadily from $[\text{O}/\text{Fe}]$ near -1.0 at $[\text{Fe}/\text{H}]$ near -3.5 to 0.0 near $[\text{Fe}/\text{H}] = 0.0$. The slope of the fit between the two parameters is -0.30 ± 0.03 . The $[\text{O}/\text{Fe}]$ enhancement diminishes steadily rather than showing a constant

enhancement below $[\text{Fe}/\text{H}]$ of -2.0 of 0.7 ± 0.17 as found by Cayrel et al. (2004).

We are grateful to the various Support Astronomers and Observing Assistants who helped us over the 11 observing runs for this project. We acknowledge support from NSF through grant AST 05-05899 to A.M.B.

REFERENCES

- Alibes, A., LaBay, J. and Ramon, C. 2002, ApJ, 571, 326
- Asplund, M. & Garc'ia Pérez, 2001, A&A, 372, 601
- Balachandran, S.C. & Bell, R.A. 1998, Nature, 392, 791
- Boesgaard, A. M. 2000, IAU symp. 198, 389
- Boesgaard, A. M. 2001, NewAr, 45, 525
- Boesgaard, A. M. 2004, in the Origin and Evolution of the Elements ed. A. McWilliam & M. Rauch, (Cambridge: Cambridge University Press), p. 117
- Boesgaard, A. M., 2007, ApJ, 667, 1196
- Boesgaard, A. M., Deliyannis, C. P., King, J. R., Ryan, S. G., Vogt, S. S., Beers, T. C. 1999a, AJ, 117, 1549
- Boesgaard, A. M., King, J. R., Deliyannis, C. P., Vogt, S. S., 1999b, AJ, 117, 492
- Boesgaard, A.M., Levesque, E.M. & Rich, J.A. 2008, First Stars III, ed. B.W. O'Shea, A Heger & T. Abel [AIP: Melville NY], p. 164
- Boesgaard, A. M. & Novicki, M. C., 2006, ApJ, 641, 1122
- Boyd, R. N. and Kajino, T., 1989, ApJ, 336, L55
- Carney, B. 1983, AJ, 83, 623
- Cayrel R., Depagne, E., Spite, M., Hill, V., Spite, F., Francois, P. et al. 2004, A&A, 416, 1117
- Duncan, D.K., Primas, F., Rebull, L.M., Boesgaard, A.M., Deliyannis, C.P., Hobbs, L.M., King, J.R. & Ryan, S.G. 1997, ApJ, 488, 338
- Fields, B. D., and Daigne, F., Casse, M., and Vangioni-Flam, E., 2002, ApJ, 581, 389
- Fulbright, J. P. & Johnson, J. A. 2003, ApJ, 595, 1154
- Garc'ia Pérez, A.E., Asplund, M., Primas, F., Nissen, P.E., & Gustafsson, B. 2006, A&A, 451, 621
- Hosford, A., Ryan, S.G., García Pérez, A.E., Norris, J.E. & Olive, K.A. 2009, A&A, 493, 601
- Israelian, G., García López, R. & Rebolo, R. 1998, ApJ, 507, 805
- Israelian, G., Rebolo, R., García López, R., Bonifacio, P., Molaro, P. Basri, G. & Shchukina, N. 2001, ApJ, 551, 833
- Jedamzik, K. and Rehm, J. B., 2001, PhRvD, 64, 3510

- Magain, P. 1984, A&A, 132, 208
- Malaney, R. A. and Fowler, W. A., 1989, ApJ, 345, L5
- Meneguzzi, M., Audouze, J., and Reeves, H. 1971, A&A, 15, 337
- Nakamura, K., Inoue, S., Wanajo, S., and Shigeyama, T., 2006, ApJ, 643, 115
- Orito, M., Kajino, T., Boyd, R. N., and Mathews, G. J., 1997, ApJ, 488, 515
- Parizot, E., 2000, A&A 362, 786
- Pasquini, L., Galli, D., Gratton, R. G., Bonifacio, P., Randich, S., Valle, G. 2005, A&A, 436, L57
- Pasquini, L., Bonifacio, P., Randich, S., Galli, D., Gratton, R. G., 2004, A&A, 426, 651
- Primas, F., Asplund, M., Nissen, P. E., and Hill, V., 2000a, A&A, 364, L42
- Primas, F., Molaro, P., Bonifacio, P. and Hill, V., 2000b, A&A, 362, 666
- Reeves, H., Fowler, W.A. and Hoyle, F. 1970, Nature, 226, 727
- Smiljanic, R., Pasquini, L., Bonifacio, P., Galli, D., Gratton, R.G., Randich, S. & Wolff, B. 2009, A&A, 499, 103
- Snedden, C. A. 1973, Ph.D. thesis, Univ. Texas, Austin
- Spergel, D. N., Bean, R., Doré, R., Nolta, M. R., Bennett, C. L. et al. 2007, ApJS, 170, 377
- Spite, F., and Spite, M. 1982, A&AS, 115, 357
- Stephens, A., 1999, A&A, 117, 1771
- Stephens, A. & Boesgaard, A. M. 2002, AJ, 123, 1647
- Suzuki, T.K. & Yoshii, Y. 2001, ApJ, 549, 303
- Tan, K.F., Shi, J.R., & Zhao, G. 2009, MNRAS, 392, 205
- Thévenin, F. & Idiart, T.P. 1999, ApJ, 521, 753
- Thomas, D., Schramm, D., Olive, K., Mathews, G., Meyer, B. S. & Fields, B.D. 1994, ApJ, 430, 291
- Vogt, S. S. et al., SPIE, 2198, 362

Table 1. Log of the Beryllium Observations

Star	Code ^a	R.A.	Dec.	V	Date(s) U.T.	Exp. min.	S/N
LP 651-4	1	02 44	−05 26	12.04	2006 Jan 2	65	83
G 75-56	2	03 00	−05 57	11.94	2004 Sep 7 2004 Nov 7	232	107
LP 831-70	3	03 06	−22 19	11.40	2008 Jan 16	90	52
BD +3 740	4	05 01	+04 06	9.80	2004 Nov 7	60	166
G 108-58	5	07 10	−01 17	11.82	2008 Jan 16	90	91
G 88-10	6	07 10	+24 20	11.86	2007 Nov 19 2008 Jan 16	150	121
BD +20 2030	7	08 16	+19 41	11.20	2006 Jan 2	60	122
BD +9 2190	8	09 29	+08 38	11.16	2005 Jan 31	120	110
BD +1 2341p	9	09 40	+01 00	10.48	2006 Jan 2	40	139
BD +44 1910	10	09 49	+44 17	10.95	2008 Jan 16	60	112
BD −13 3442	11	11 46	−14 06	10.37	2006 Jan 2	80	194
LP 553-62	12	11 54	+02 57	11.68	2008 Jan 16	90	97
G 11-44	13	12 10	+00 23	11.08	2008 Jan 16	30	76
G 59-24	14	12 34	+15 16	12.02	2008 Jan 16	56	73
G 64-12	15	13 40	−00 02	11.49	2005 May 15	210	109
G 64-37 ^b		14 02	−05 39	11.14	2003 May 27	270	87
G 201-5	16	14 36	+55 33	11.52	2007 Jun 10	120	115
BD +26 2621	17	14 54	+25 33	11.00	2007 Jun 10	60	123
G 206-34	18	18 35	+28 41	11.40	2005 May 15	105	97
LP 752-17	19	19 25	−11 56	11.88	2005 Jul 6 2005 Sep 27 2006 Jun 19	240	94
G 92-6	20	19 29	+01 01	11.75	2007 Jun 10	120	100
LP 635-14	21	20 26	−00 37	11.33	2005 Jul 6 2007 Jun 10	162	114
LP 815-43	22	20 38	−20 25	10.91	2004 Sep 7 2006 Jun 19	120	98
G 275-4	23	23 07	−23 52	12.18	2005 Jul 5 2005 Jul 6 2005 Sep 27	220	61

^aCode is an ID number for the star in the Appendix Table of equivalent widths.

^bG64-37 observed on Subaru with HDS. See Boesgaard & Novicki (2006).

Table 2. Lines Measured

Element	$\lambda(\text{\AA})$	Ex. Pot.(eV)	gf
Fe I	3100.304	0.99	0.1348963
	3100.665	0.95	0.1361445
	3116.631	1.01	0.0221309
	4494.563	2.1980	0.0725270
	4528.614	2.1760	0.1297180
	4531.148	1.4850	0.0074470
	4556.126	3.6030	0.1633050
	4592.651	1.5580	0.0035030
	4602.941	1.4850	0.0061940
	4647.434	2.9490	0.0467200
	4678.846	3.6030	0.1792670
	4691.411	2.9910	0.0326210
	4733.591	1.4850	0.0010300
	4736.773	3.2110	0.1794730
	4871.318	2.8660	0.4111500
	4872.137	2.8820	0.2609160
	4890.750	2.8600	0.4036454
	4891.490	2.8400	0.7744618
	4918.994	2.8660	0.4405550
	4920.503	2.8330	1.1587773
	4985.253	3.9290	0.2760580
	4985.547	2.8650	0.0466660
	4994.130	0.9150	0.0010740
	5001.862	3.8820	1.0232930
	5006.119	2.8330	0.2298790
	5012.068	0.8590	0.0023820
	5022.236	3.9840	0.2951210
	5049.819	2.2790	0.0447200
	5051.635	0.9150	0.0017220
	5068.766	2.9400	0.0731980
	5079.224	2.1980	0.0082040
	5079.740	0.9900	0.0005850
	5083.339	0.9580	0.0014390

Table 2—Continued

Element	$\lambda(\text{\AA})$	Ex. Pot.(eV)	gf
	5098.697	2.1760	0.0094190
	5123.720	1.0110	0.0008650
	5150.840	0.9900	0.0009550
	5171.596	1.4850	0.0174985
	5192.344	2.9980	0.3793150
	5194.942	1.5580	0.0088000
	5198.711	2.2230	0.0077090
	5202.336	2.1760	0.0139800
	5215.182	3.2660	0.1345860
	5216.274	1.6080	0.0076560
	5217.390	3.2110	0.0765600
	5227.190	1.5570	0.0592925
	5232.940	2.9400	0.8016780
	5242.491	3.6350	0.1248820
	5250.646	2.1980	0.0076740
	5263.305	3.2660	0.1189870
	5269.537	0.8590	0.0475883
	5328.039	0.9150	0.0342373
	5332.900	1.5570	0.0013870
	5339.930	3.2660	0.2089300
	5341.024	1.6080	0.0098510
	5393.167	3.2410	0.1539930
	5397.128	0.9150	0.0102920
	5405.775	0.9900	0.0140605
	5429.696	0.9580	0.0131825
	5434.524	1.0110	0.0075510
	5455.609	1.0110	0.0080445
	5497.516	1.0110	0.0014550
	5501.465	0.9580	0.0010050
	5569.618	3.4170	0.3069020
	5572.841	3.3970	0.5099180
	5576.090	3.4300	0.1000000
	5586.756	3.3680	0.7177940

Table 2—Continued

Element	$\lambda(\text{\AA})$	Ex. Pot.(eV)	gf
	5658.816	3.3970	0.1458810
Fe II	4508.289	2.8580	0.0047753
	4515.339	2.8440	0.0033113
	4522.634	2.8440	0.0077625
	4576.339	2.8410	0.0011092
	4583.837	2.8070	0.0120226
	4629.339	2.8070	0.0042658
	5197.576	3.2310	0.0068155
	5234.630	3.2210	0.0061660
	5276.002	3.2000	0.0092257
Ti I	4518.023	0.8259	0.5382698
	4527.305	0.8130	0.3388442
	4533.239	0.8484	3.4040819
	4534.778	0.8360	2.1677041
	4535.570	0.8259	1.3182567
	4681.908	0.0480	0.0966051
	4981.732	0.8484	3.6307805
	4991.067	0.8360	2.7289778
	4999.504	0.8259	2.0230192
	5016.162	0.8484	0.3033891
	5020.028	0.8360	0.4385307
	5022.871	0.8259	0.4187936
	5035.907	1.4602	1.8197009
	5036.468	1.4432	1.5346170
	5039.959	0.0211	0.0741310
	5064.654	0.0480	0.1396368
Ti II	4501.272	1.1156	0.1757924
	4501.272	1.1156	0.1757924
	4563.761	1.2214	0.1096478
	4571.968	1.5719	0.2951209

Table 2—Continued

Element	$\lambda(\text{\AA})$	Ex. Pot.(eV)	gf
	4589.958	1.2369	0.0162181
	4657.203	1.2430	0.0058210
	4779.985	2.0478	0.0426580
	5129.152	1.8918	0.0407380
	5154.070	1.5659	0.0120226
	5188.680	1.5819	0.0616595
	5226.543	1.5659	0.0501187
	5336.781	1.5819	0.0216272
	5381.018	1.5658	0.0094406

Table 3. Stellar Parameters and Abundances

Star	T_{eff} (K)	$\log g$	[Fe/H]	$\sigma([\text{Fe}/\text{H}])^{\text{a}}$	[O/H]	$\sigma([\text{O}/\text{H}])$	A(Be)	$\sigma(\text{Be})$
LP 651-4	6030	4.26	-2.89	0.08	-2.04	0.14	-1.12	0.12
G 75-56	5890	3.83	-2.38	0.08	-1.74	0.14	-0.84	0.12
LP 831-70	5985	4.75	-3.06	0.11	-2.45	0.13	< -0.90	0.12
BD +3 740	6030	3.83	-2.95	0.09	-2.26	0.14	-1.40	0.11
G 108-58	5865	4.03	-2.37	0.10	-1.33	0.15	-1.12	0.12
G 88-10	5945	4.00	-2.61	0.07	-1.86	0.15	-1.08	0.12
BD +20 2030	5978	3.61	-2.77	0.10	-2.06	0.14	-1.23	0.12
BD +9 2190	6008	3.85	-3.00	0.09	-2.38	0.14	-1.22	0.11
BD +1 2341p	6402	4.24	-2.67	0.11	-1.76	0.14	-1.00	0.12
BD +44 1910	5878	3.56	-2.64	0.08	-1.96	0.15	-1.11	0.12
BD -13 3442	6090	4.11	-2.91	0.09	-2.15	0.15	-1.12	0.12
LP 553-62	6128	3.93	-2.73	0.08	-2.02	0.14	-1.00	0.11
G 11-44	5820	3.58	-2.29	0.05	-1.63	0.15	-1.04	0.11
G 59-24	6112	4.10	-2.32	0.10	-1.32	0.15	-0.69	0.11
G 64-12	6074	3.72	-3.45	0.04	-2.24	0.15	-1.43	0.12
G 64-37	6122	3.87	-3.28	0.05	-2.32	0.14	-1.40	0.11
G 201-5	5950	4.00	-2.54	0.08	-1.97	0.15	-1.27	0.11
BD +26 2621	6266	4.50	-2.69	0.09	-1.96	0.13	-0.94	0.11
G 206-34	5825	3.99	-3.12	0.09	-2.37	0.14	-1.20	0.11
LP 752-17	5738	3.20	-2.38	0.08	-1.80	0.17	-0.86	0.12
G 92-6	6115	4.79	-2.70	0.08	-2.28	0.12	-0.91	0.11
LP 635-14	5932	3.57	-2.71	0.07	-2.00	0.12	-1.17	0.12
LP 815-43	6405	4.37	-2.76	0.11	-1.86	0.15	-0.95	0.12
G 275-4	5942	4.05	-3.42	0.09	-2.48	0.15	-1.53	0.11

^aThese are t

Table 4. New Beryllium and Oxygen Abundances from Boesgaard et al. (1999a)

Star	T_{eff} (K)	σ	log g	σ	[Fe/H]	σ	[O/H]	σ	A(Be)	σ
HD 19445	5853	40	4.41	0.23	-2.10	0.12	-1.53	0.10	-0.48	0.06
HD 64090	5500	40	4.73	0.10	-1.77	0.18	-1.36	0.07	-0.09	0.13
HD 74000	6134	40	4.26	0.10	-2.05	0.12	-1.56	0.06	-0.49	0.06
HD 76932	5807	40	4.00	0.12	-0.95	0.11	-0.65	0.08	+0.77	0.05
HD 84937	6206	40	3.89	0.13	-2.20	0.14	-1.49	0.05	-0.83	0.07
HD 94028	5907	64	4.44	0.17	-1.54	0.09	-1.17	0.10	+0.39	0.08
HD 134169	5759	82	3.68	0.16	-0.94	0.05	-0.66	0.10	+0.55	0.10
HD 140283	5692	40	3.47	0.13	-2.56	0.12	-1.72	0.06	-1.18	0.09
HD 184499	5670	40	4.00	0.15	-0.51	0.14	-0.41	0.08	+1.12	0.09
HD 194598	5911	42	4.32	0.13	-1.25	0.16	-1.06	0.07	+0.14	0.05
HD 201889	5553	41	3.74	0.24	-0.95	0.26	-1.02	0.08	+0.58	0.13
HD 219617	5872	40	4.52	0.15	-1.58	0.16	-1.27	0.08	-0.23	0.12
BD +37°1458	5500	40	3.41	0.26	-2.14	0.17	-1.14	0.09	-0.93	0.08
BD +26°3578	6158	64	3.94	0.12	-2.32	0.15	-1.69	0.06	-0.90	0.10
BD +23°3912	5691	40	3.68	0.10	-1.53	0.15	-1.17	0.06	+0.02	0.05
BD +20°3603	6114	89	4.27	0.20	-2.22	0.16	-1.66	0.12	-0.60	0.11
BD +17°4708	5956	62	3.65	0.26	-1.81	0.10	-1.31	0.09	-0.43	0.08
BD +03°740	6110	82	3.64	0.33	-2.89	0.09	-2.16	0.12	-1.37	0.10
BD +02°3375	5800	40	4.07	0.41	-2.39	0.17	-1.85	0.11	-0.74	0.15
BD -04°3208	6316	121	3.90	0.42	-2.35	0.20	-1.37	0.11	-0.72	0.15
BD -13°3442	5900	40	3.50	0.44	-3.02	0.16	-2.28	0.12	-1.70	0.21

Table 5. Other Beryllium and Oxygen Abundances from Subaru and Keck Observations

Star	T_{eff} (K)	σ	$\log g$	σ	[Fe/H]	σ	[O/H]	σ	A(Be)	σ
HD 24289 ^a	5700	100	3.50	0.50	-2.22	0.10	-1.67	0.14	-0.83	0.14
HD 233511 ^a	5900	40	4.20	0.06	-1.70	0.08	-1.23	0.14	-0.23	0.14
HD 132475 ^b	5765	62	3.60	0.20	-1.50	0.15	-0.90	0.15	+0.57	0.12
G 21-22 ^b	5916	84	4.59	0.30	-1.02	0.25	-0.98	0.15	+0.33	0.16
HD 194598 ^a	5875	40	4.2	0.06	-1.23	0.08	-1.00	0.14	+0.12	0.14
HD 195633 ^b	5986	115	3.89	0.08	-0.88	0.16	-0.67	0.15	+0.66	0.11
HD 201891 ^b	5806	110	4.42	0.20	-1.07	0.10	-0.86	0.15	+0.62	0.11

^aKeck data in Boesgaard (2007)

^bSubaru data in Boesgaard & Novicki (2006)

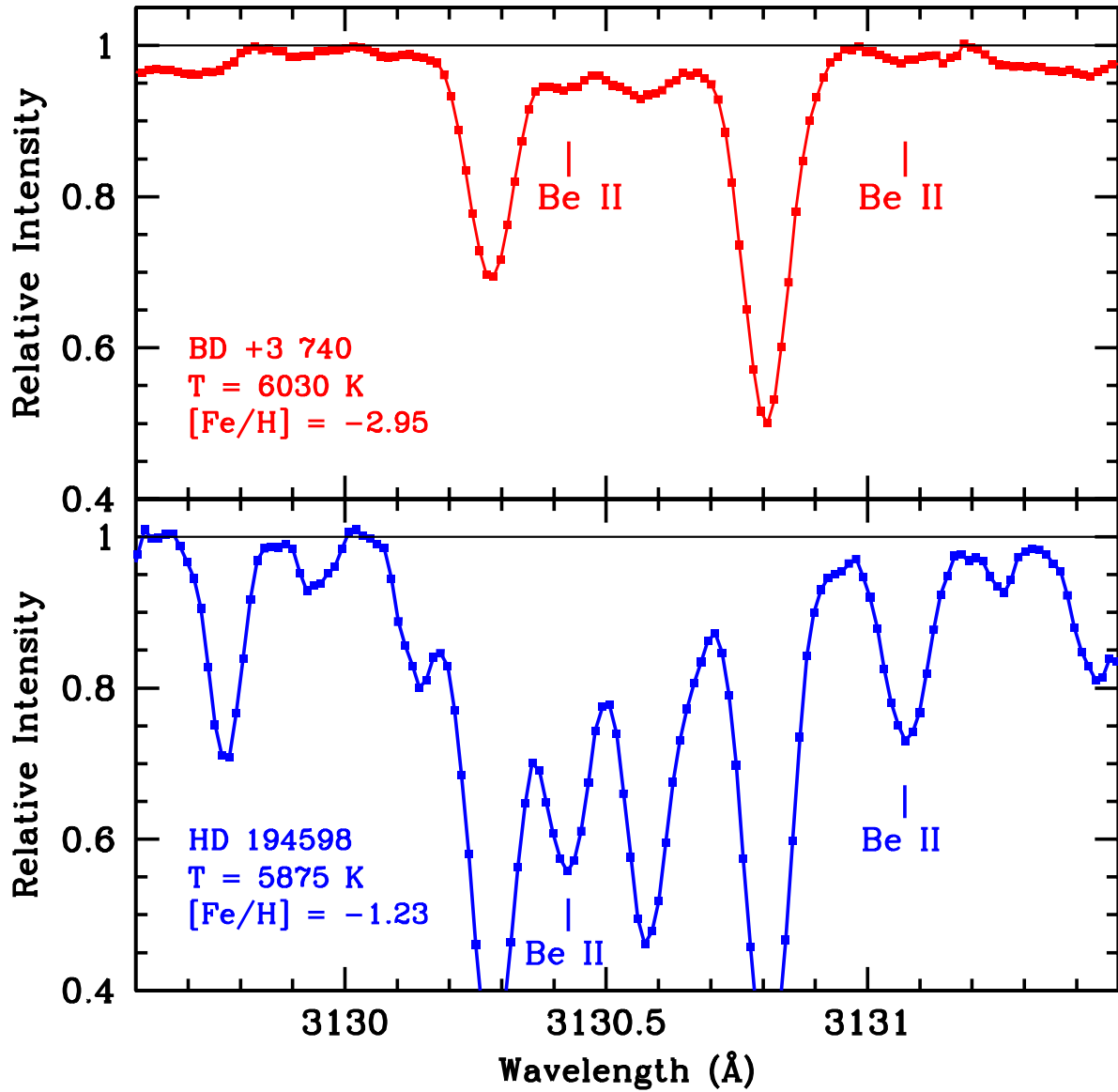


Fig. 1.— The Be region of BD +3 740 ($[\text{Fe}/\text{H}] = -2.95$) from our sample of very metal-poor stars compared to HD 194598 ($[\text{Fe}/\text{H}] = -1.23$) with much higher metallicity. Both the Be doublet and the OH feature (at 3130.6 \AA) are much reduced at low metallicities, necessitating the high signal to noise of our observations.

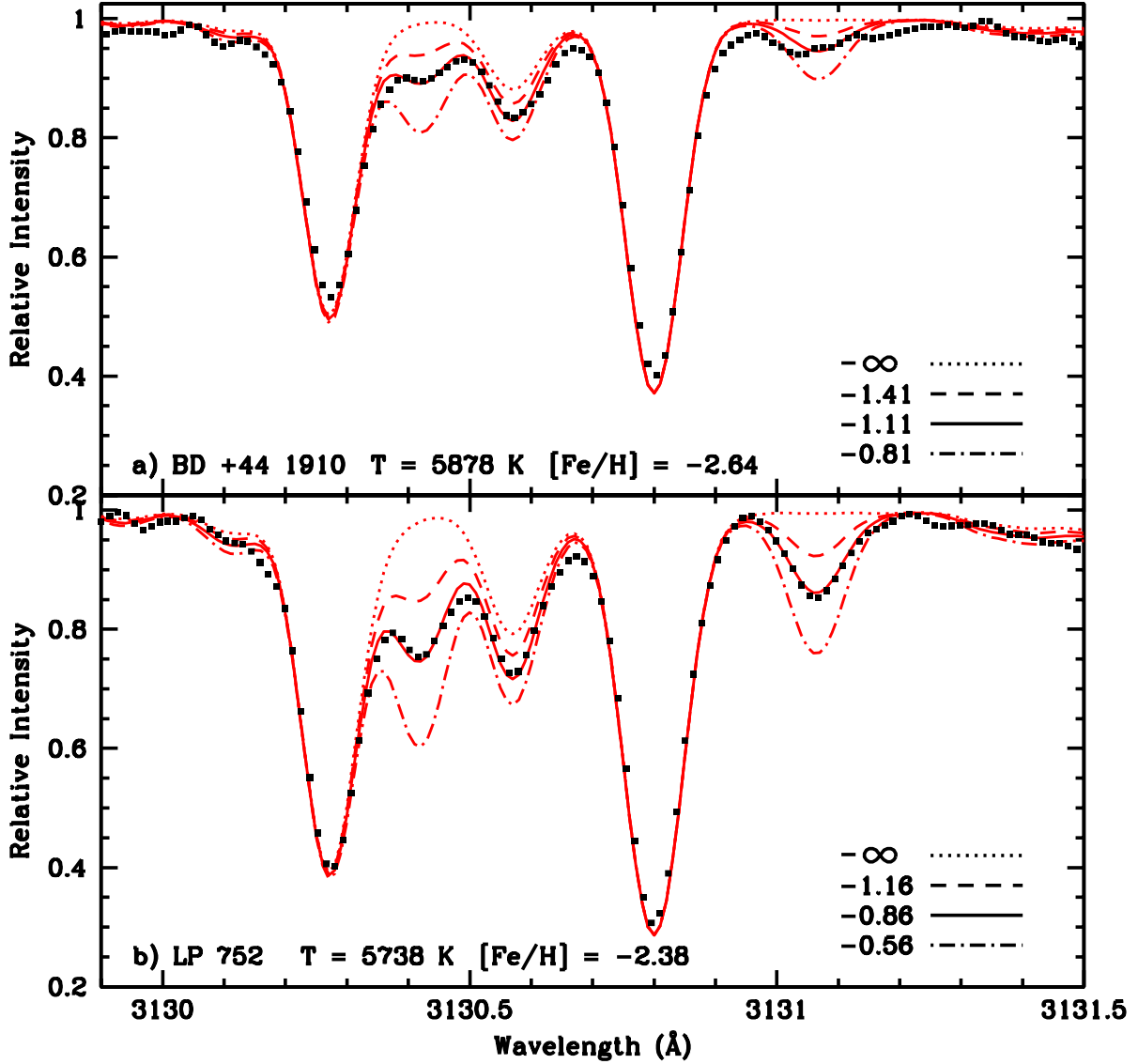


Fig. 2.— Examples of a output from MOOG’s “synth” driver. The small squares are the spectral data and the solid lines are the best fits. The dotted line represents a fit with no Be, while the dot-dash line has a factor of 2 more Be than the best fit and the dashed line has a factor of 2 less. The OH feature in the region at 3130.57 \AA is used to find the O abundance. The O abundance has also been varied by ± 0.1 dex in the models.

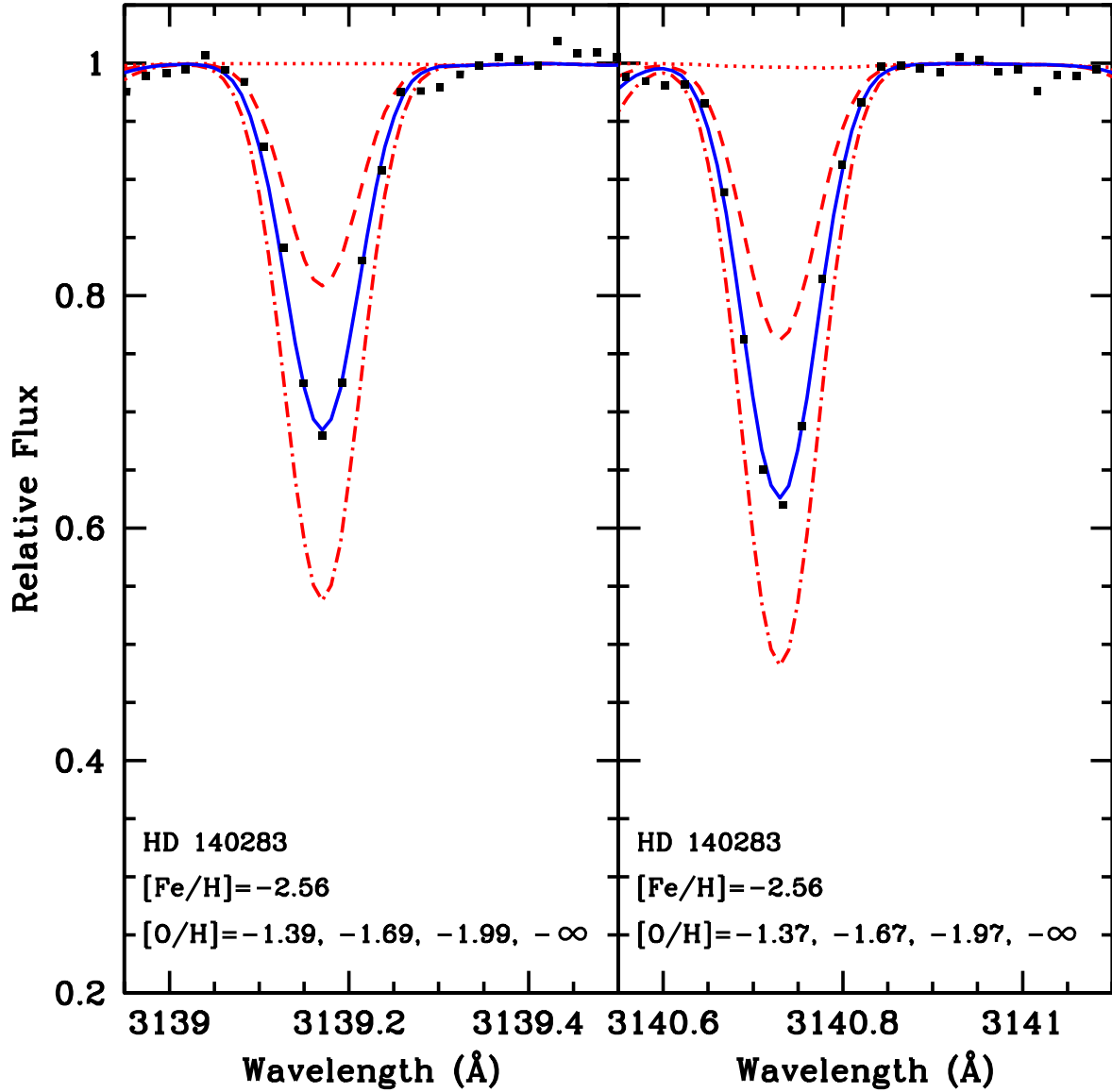


Fig. 3.— An example of the spectrum synthesis for the other two OH regions that we used to find the O abundances. The small squares are the spectral data and the solid lines are the best fits. The dot-dash line has a factor of 2 more O than the best fit and the dashed line has a factor of 2 less.

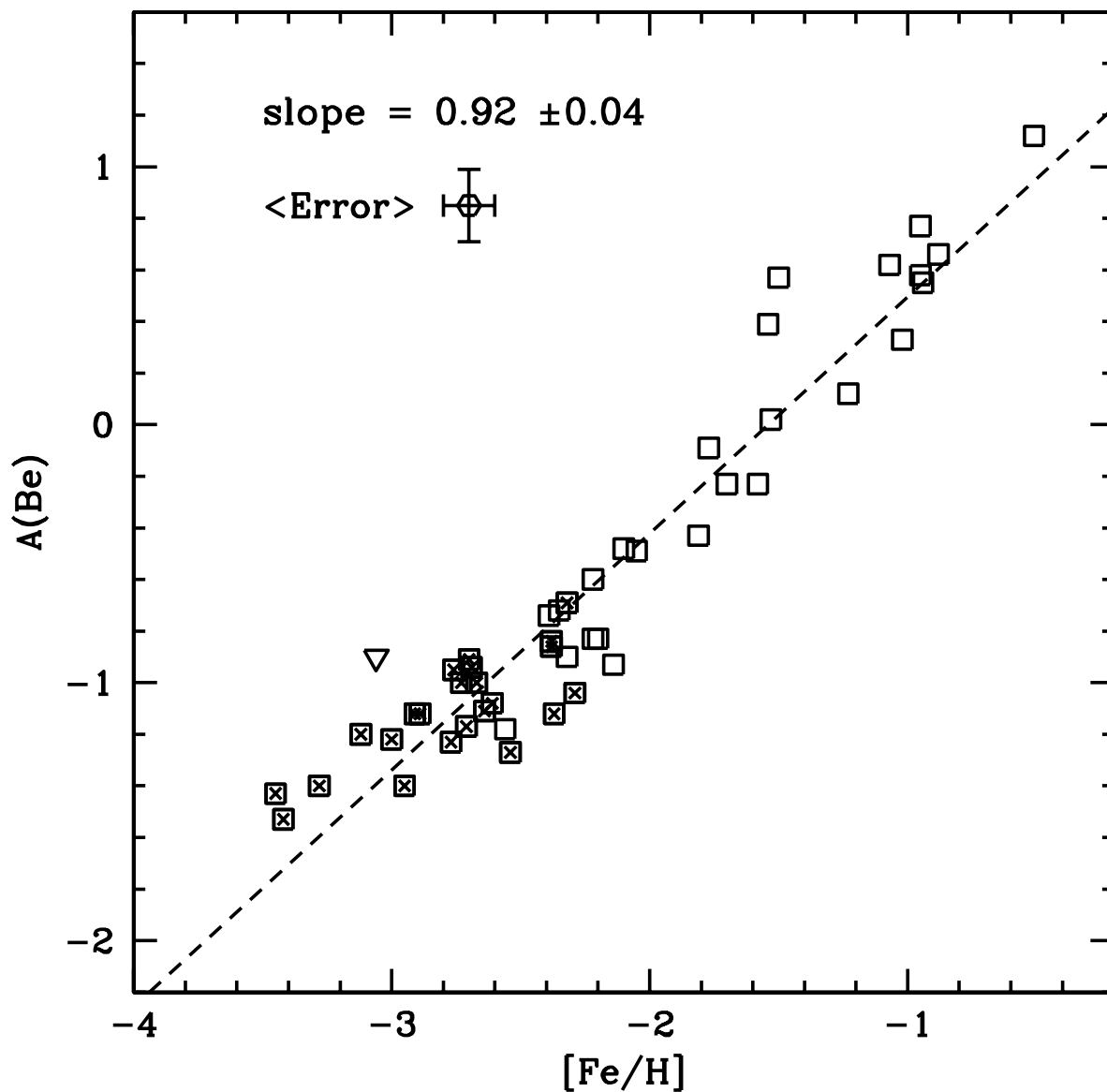


Fig. 4.— Our Be abundances versus $[\text{Fe}/\text{H}]$ along with a typical error bar. The squared crosses represent the new data in this paper while the open squares are revised values from Tables 4 and 5. The triangle is the Be upper limit for LP 831-70, which was not included in the least squares fit. The results do not seem to indicate a significant Be plateau at low metallicities, a possibility discussed in Primas et al. (2000a). The results can be represented by a single linear fit over more than 3 orders of magnitude in $[\text{Fe}/\text{H}]$ and more than 2 orders of magnitude in $A(\text{Be})$.

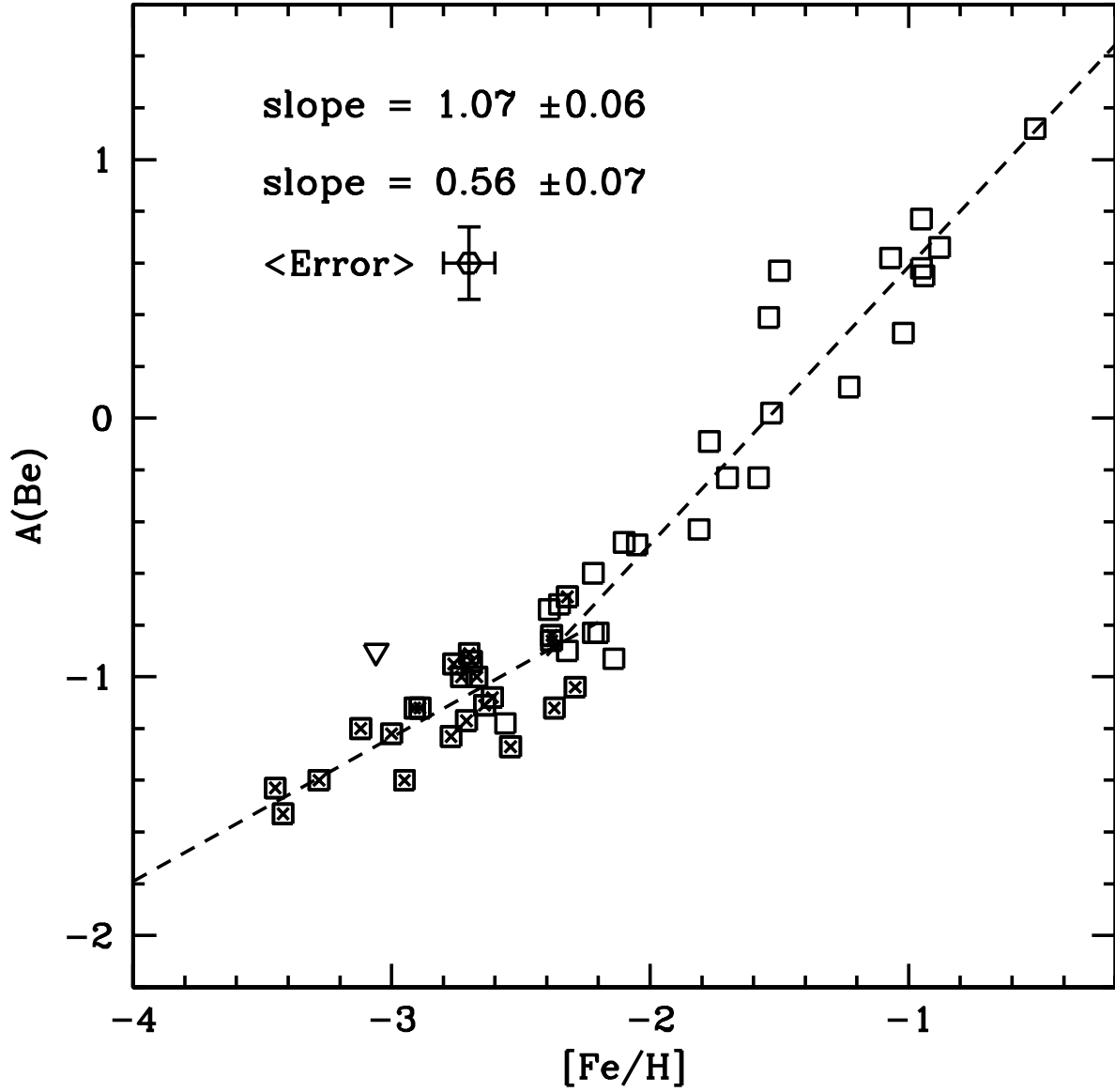


Fig. 5.— This is the same plot as Figure 4, but with a dual linear fit. This fit may be more pleasing to the eye, but there is no statistical reason to prefer it.

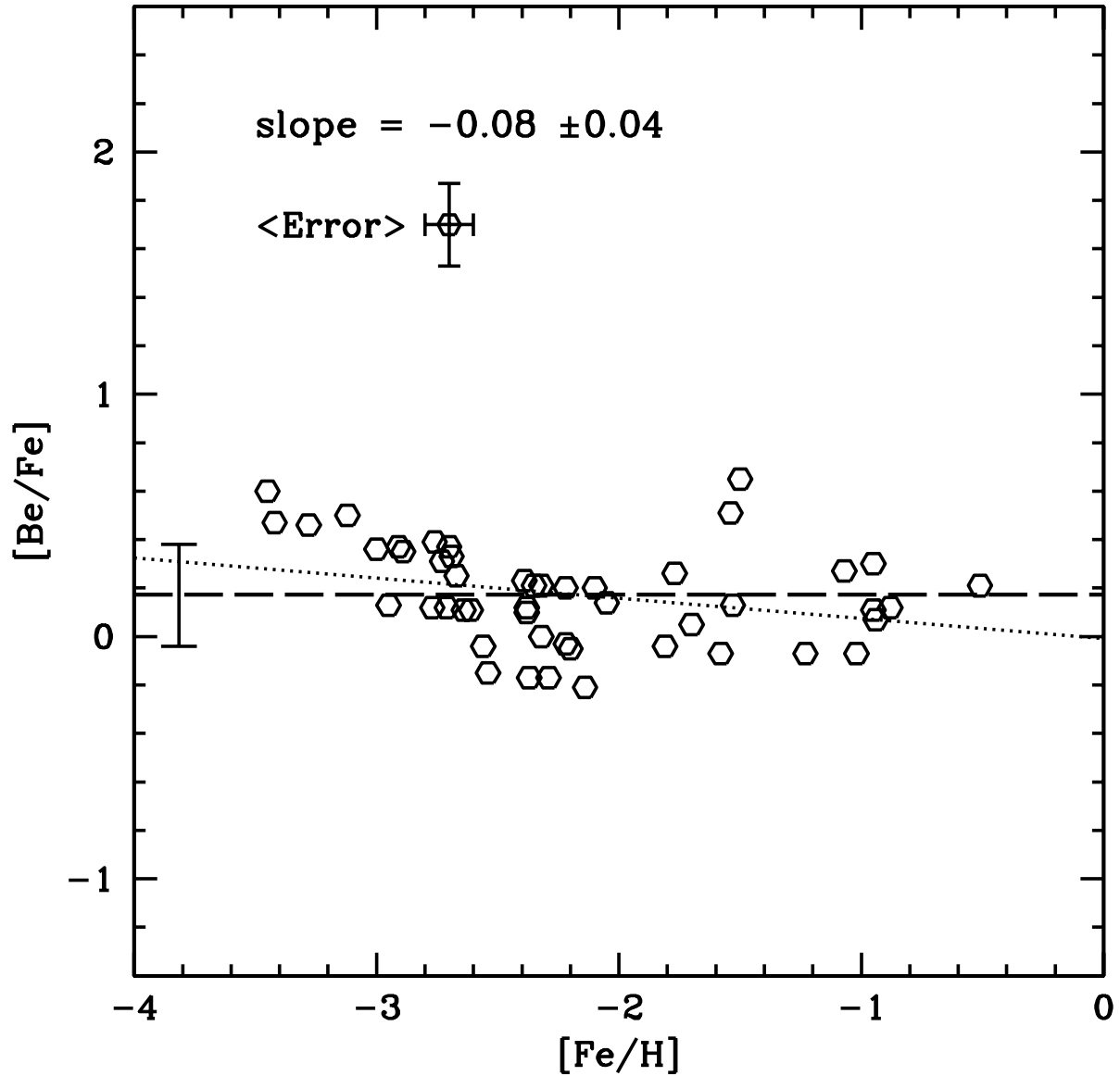


Fig. 6.— This figure shows the trend of Be as normalized to Fe, $[Be/Fe]$, compared to the Fe abundance. The dashed line is the mean value of $[Be/Fe]$, $+0.17 \pm 0.21$, and the dotted line is the best linear fit. The probable error of the mean value is shown at the left along the dashed mean line. The most metal poor stars show an upward trend in $[Be/Fe]$ toward lower $[Fe/H]$, rather than a plateau.

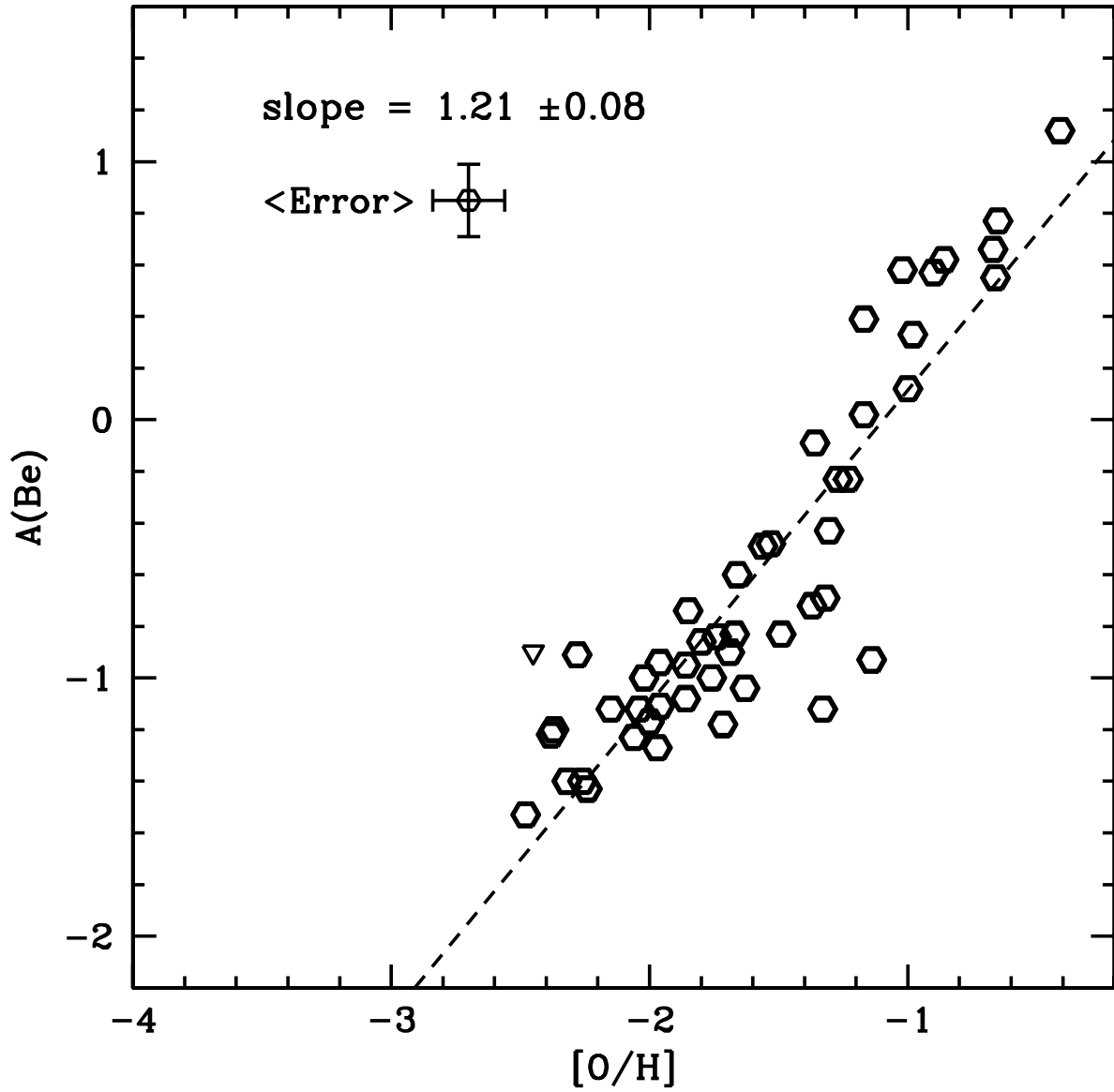


Fig. 7.— The Be abundances compared to our O abundances. The triangle is the Be upper limit for LP 831-70, which was not included in the least squares fit. A linear fit is shown between the two quantities and has a slope of 1.21 ± 0.08 . The two stars with high $[O/H]$ and/or low $A(\text{Be})$ are G 108-58 and BD +37 1458.

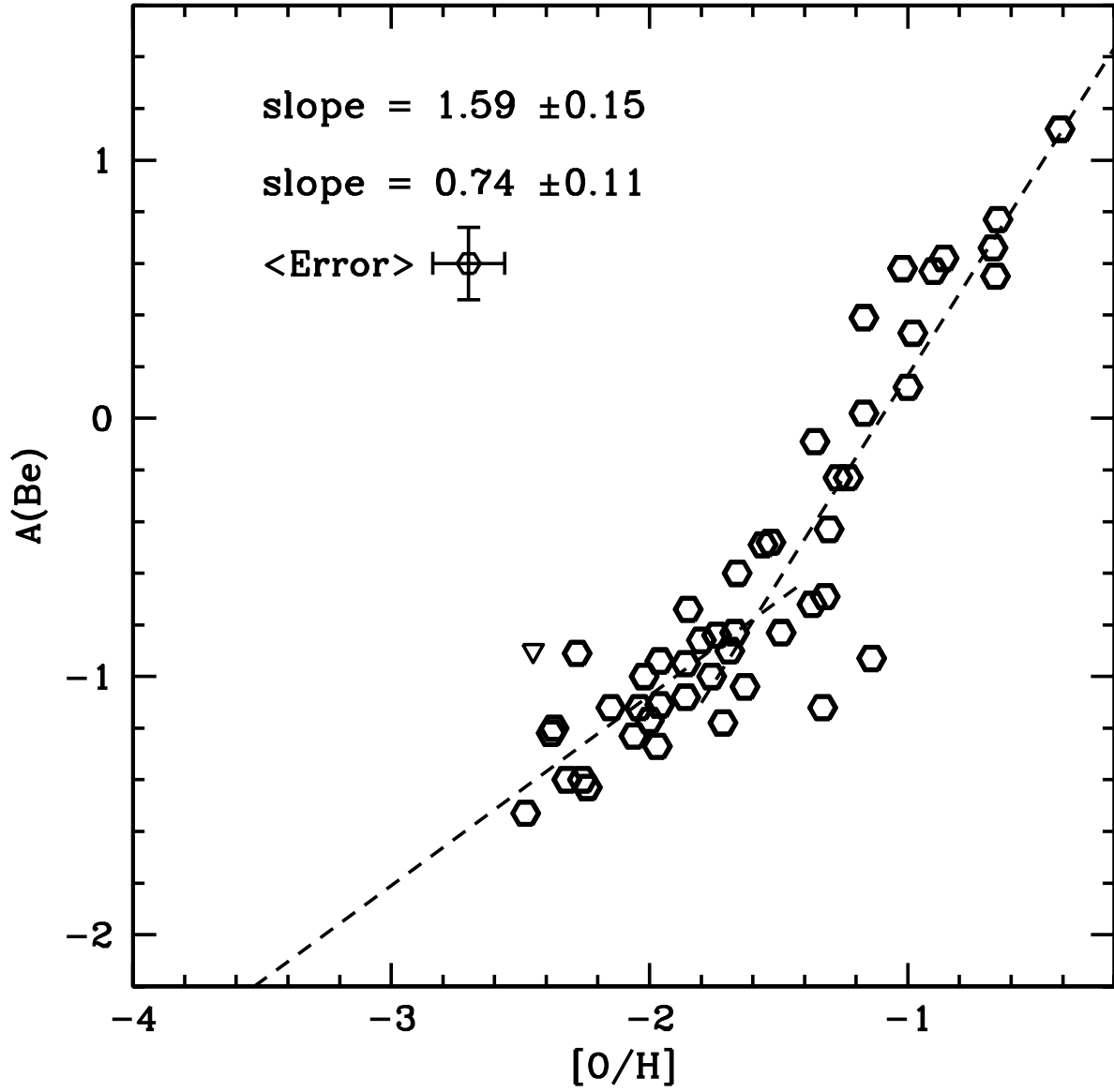


Fig. 8.— The same as Figure 7 except the data are fit with two linear relations: one for stars with $[\text{O}/\text{H}] > -1.8$ and the other for stars with $[\text{O}/\text{H}] < -1.4$. The transition seems to occur at $[\text{O}/\text{H}]$ near -1.6 , corresponding to $[\text{Fe}/\text{H}] \sim -2.2$.

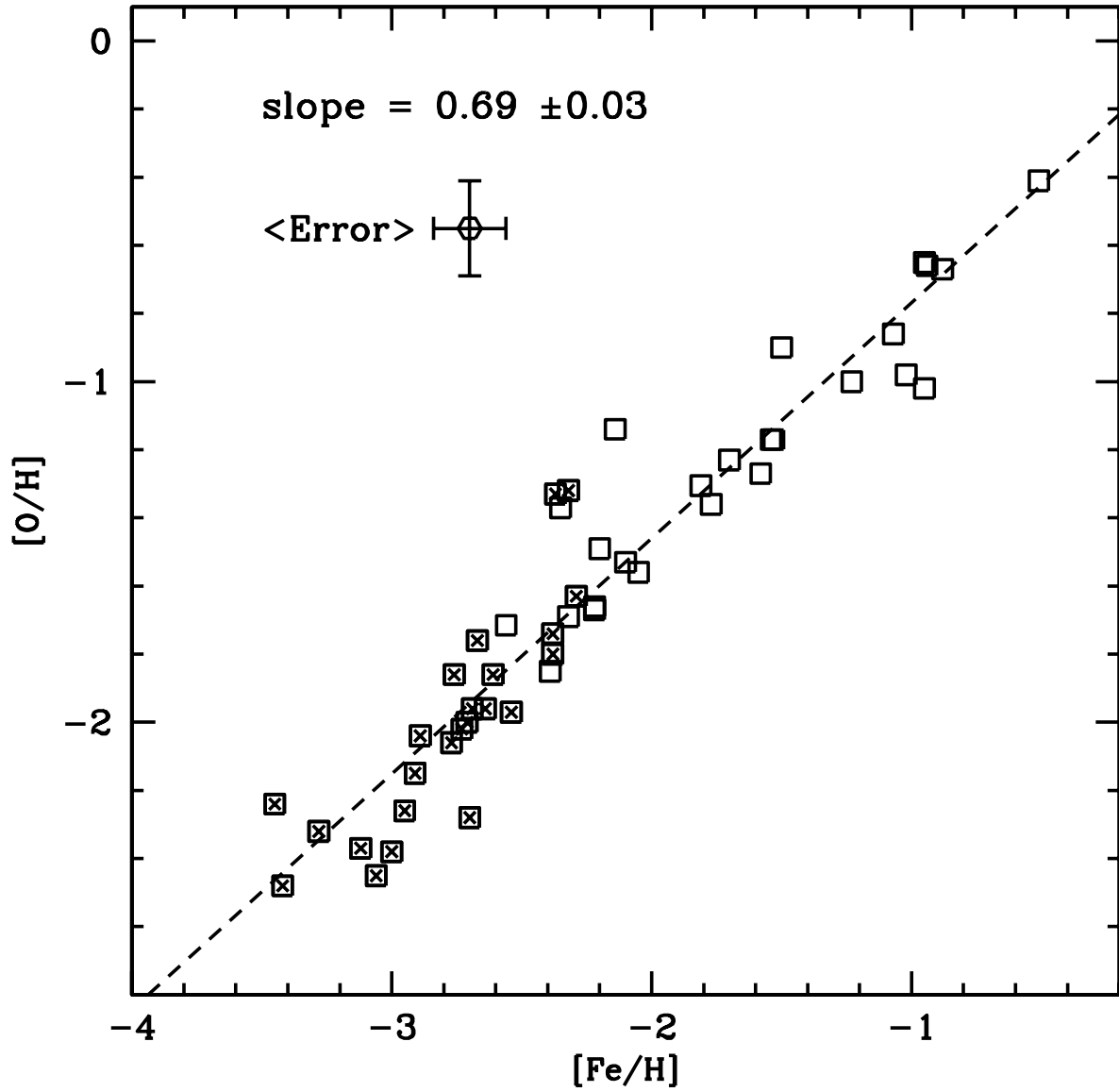


Fig. 9.— The tight linear relationship between O and Fe. The fit is good over the 3+ orders of magnitude in Fe and 2+ orders of magnitude in O. The squared crosses are the new data from Table 3 and the open squares are the data from Tables 4 and 5. The data sets merge well with each other.

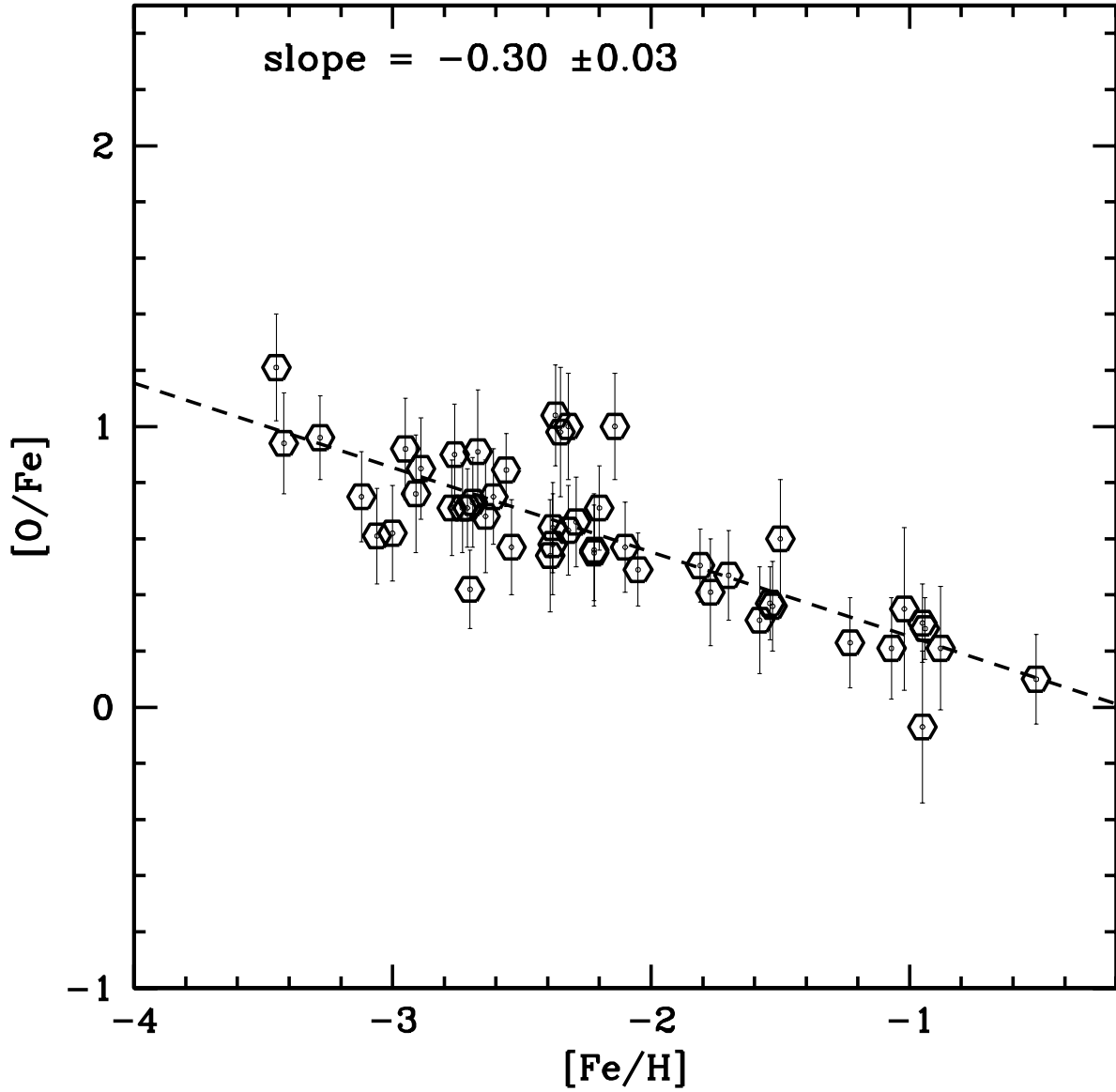


Fig. 10.— This is a standard plot showing the enhancement of O relative to Fe in low metal stars. It indicates that the O enhancement diminishes steadily reaching $[O/Fe] = 0.0$ at $[Fe/H] = 0.0$. In this Figure we show the individual error bars on $[O/Fe]$.

6. Appendix

Table 6a. Measured Equivalent Widths

λ (Å)	Ele.	1	2	3	4	5	6	7	8	9	10	11	12
3100.304	Fe I	41.9	41.5	...	44.8	...
3100.665	Fe I	46.4	43.3
3116.631	Fe I	20.0	...	22.2	16.3	...	34.7	...	17.6	15.8	...	20.4	20.1
4494.563	Fe I	12.7	31.8	8.3	11.7	...	24.1	15.8	11.2	11.3	20.6	11.0	15.5
4528.614	Fe I	24.6	...	17.4	20.1	...	36.9	29.0	18.1	23.0	...	21.0	26.1
4531.148	Fe I	6.4	16.2	6.1	6.1	19.7	11.3	9.6	7.4	6.8	16.1	5.9	7.0
4556.126	Fe I	6.5	5.8
4592.651	Fe I	12.3	8.2
4602.941	Fe I	4.6	16.4	...	4.2	20.3	12.7	7.9	6.4	6.3	12.7	5.3	8.6
4647.434	Fe I	6.0	7.6
4678.846	Fe I	7.0
4691.411	Fe I	5.7
4733.591	Fe I	5.3
4736.773	Fe I	5.3
4871.318	Fe I	16.7	14.3	14.3	10.9	7.9	...	4.9	9.9	4.9	6.5
4872.137	Fe I	12.9	28.2	8.6	7.6	27.9	19.0	12.8	8.5	9.2	17.4	9.9	12.2
4890.750	Fe I	16.3	34.3	10.9	14.1	...	25.9	20.4	11.5	17.3	24.1	14.0	17.6
4891.490	Fe I	25.9	...	18.5	21.4	...	38.3	29.0	20.7	26.3	...	23.2	26.8
4918.994	Fe I	17.6	...	13.4	13.9	...	31.2	19.2	12.0	15.4	26.7	14.5	20.7
4920.503	Fe I	32.1	...	27.2	31.4	...	46.7	...	31.9	31.3	...	29.0	...
4985.253	Fe I	5.7
4985.547	Fe I	6.9
4994.130	Fe I	15.0
5001.862	Fe I	14.1
5006.119	Fe I	9.7	25.8	7.9	10.6	28.9	20.5	13.2	11.4	9.6	18.2	6.7	13.0
5012.068	Fe I	10.2	23.0	7.4	9.7	30.9	16.7	10.9	7.5	7.4	19.2	6.9	10.1
5022.236	Fe I	6.3
5049.819	Fe I	22.4
5051.635	Fe I	24.2
5068.766	Fe I	10.5
5079.224	Fe I	8.2
5079.740	Fe I	8.2

Table 6a—Continued

λ (Å)	Ele.	1	2	3	4	5	6	7	8	9	10	11	12
5083.339	Fe I	15.3
5098.697	Fe I	11.4
5123.720	Fe I	3.2	7.9	11.9	7.1	4.4
5150.840	Fe I	11.4
5171.596	Fe I	13.9	33.1	8.9	17.7	...	34.0	16.6	12.6	10.8	24.2	13.0	17.4
5192.344	Fe I	10.1	27.5	8.9	11.4	30.1	20.6	12.7	8.6	11.6	19.1	8.9	13.7
5194.942	Fe I
5198.711	Fe I	8.0
5202.336	Fe I	13.1
5215.182	Fe I	7.4
5216.274	Fe I	20.1
5217.390	Fe I	6.2
5227.190	Fe I	32.5	...	22.8	30.7	...	50.2	...	28.0	25.6	...	30.0	36.6
5232.940	Fe I	23.0	...	15.2	20.9	...	37.1	27.9	19.2	18.6	35.4	19.4	25.8
5242.491	Fe I	5.2
5250.646	Fe I	6.8
5263.305	Fe I	8.5
5269.537	Fe I	51.2	57.6	...	77.2	...	53.7	54.2	...	59.0	...
5328.039	Fe I	43.1	49.0	...	68.5	...	45.0	44.7	...	50.4	...
5332.900	Fe I	5.1
5339.930	Fe I	14.9
5341.024	Fe I	...	27.7	11.9	9.2	28.0	18.7	...	5.9	10.2	19.7	10.9	11.6
5393.167	Fe I	11.3
5397.128	Fe I	25.4	...	19.1	23.5	...	41.5	32.7	22.7	20.5	...	22.4	29.4
5405.775	Fe I	28.8	...	21.7	31.2	...	45.7	35.2	24.5	23.1	...	26.1	31.6
5429.696	Fe I	29.8	...	22.3	26.8	...	46.9	...	25.3	26.9	...	26.1	32.8
5434.524	Fe I	17.4	...	12.4	22.	36.5	30.8	24.2	12.3	12.5	30.8	15.7	20.0
5455.609	Fe I	19.1	...	15.2	18.6	...	34.6	28.6	17.1	16.1	35.2	16.3	25.4
5497.516	Fe I
5501.465	Fe I
5569.618	Fe I	12.0
5572.841	Fe I	5.8	20.6	5.1	6.2	20.7	15.3	11.8	...	7.0	13.8	6.6	10.7
5576.090	Fe I	8.3

Table 6a—Continued

λ (Å)	Ele.	1	2	3	4	5	6	7	8	9	10	11	12
5586.756	Fe I	...	29.9	8.6	12.2	30.9	21.5	17.6	10.8	9.8	17.9	12.0	14.7
5658.816	Fe I	8.3
4508.289	Fe II	6.1	17.2	5.3	7.7	9.6	10.8	9.5	6.3	8.6	12.1	6.5	10.5
4515.339	Fe II	5.5	14.8	5.7	5.5	8.2	10.4	8.4	4.9	5.4	9.5	5.9	9.6
4522.634	Fe II	10.3	24.6	7.1	11.2	13.9	14.9	13.3	13.4	10.1	16.7	9.5	15.1
4576.339	Fe II	...	6.5	5.0
4583.837	Fe II	17.6	...	9.6	21.4	25.1	27.8	23.4	21.0	18.5	28.4	20.7	26.8
4629.339	Fe II	7.4	18.6	6.4	6.9	9.1	10.8	8.9	7.5	7.0	12.0	6.6	9.8
5197.576	Fe II	4.7	13.5	...	4.2	6.1	6.7	6.5	4.8	5.7	6.6	4.8	6.1
5234.630	Fe II	3.6	15.3	...	5.8	7.7	9.2	7.5	4.0	5.8	9.2	5.3	8.7
5276.002	Fe II	4.5	18.6	...	8.3	8.2	10.7	8.3	8.5	7.0	11.9	7.0	9.2
4518.023	Ti I	...	5.1	5.0
4527.305	Ti I
4533.239	Ti I	9.7	19.5	5.3	8.8	16.3	13.0	10.4	8.4	9.3	16.6	9.3	11.9
4534.778	Ti I	...	16.5	...	5.9	12.0	13.6	6.5	6.4	4.5	9.7	10.4	10.6
4535.570	Ti I	...	12.6	...	4.7	9.0	8.7	4.9	5.1	...	5.3	7.7	9.5
4681.908	Ti I	...	5.9	5.6	...	3.6	5.9
4981.732	Ti I	12.9	23.8	5.6	13.6	18.0	17.9	12.4	8.5	8.5	16.9	11.8	14.2
4991.067	Ti I	13.2	23.5	10.9	7.1	17.9	13.8	15.6	5.7	11.2	20.1	13.9	11.9
4999.504	Ti I	7.8	15.9	12.1	13.1	8.6	5.9	5.7	11.0	7.2	9.9
5016.162	Ti I	...	3.6
5020.028	Ti I	...	7.5	5.3	5.2
5022.871	Ti I
5035.907	Ti I
5036.468	Ti I	...	5.9
5039.959	Ti I	...	6.4
5064.654	Ti I	...	5.8	3.2	5.4
4501.272	Ti II	17.5	40.4	...	47.9	...	35.6	34.6	...	43.1	...
4563.761	Ti II	29.9	...	14.0	33.8	...	40.7	...	27.5	27.9	...	33.9	...
4571.968	Ti II	17.2	40.8	...	45.7	...	34.8	34.9	...	41.0	...

Table 6b—Continued

λ (Å)	Ele.	13	14	15	16	17	18	19	20	21	22	23
5098.697	Fe I
5123.720	Fe I	5.8	13.1	...	6.5
5150.840	Fe I	...	7.5
5171.596	Fe I	17.4	31.6	5.5	27.2	13.3	12.5	...	17.5	20.6	8.0	6.8
5192.344	Fe I	13.7	23.8	...	23.3	11.0	8.6	33.2	13.3	18.7	6.4	6.8
5194.942	Fe I	...	17.8
5198.711	Fe I	...	5.3
5202.336	Fe I	...	10.3
5215.182	Fe I	...	6.4
5216.274	Fe I	...	13.0
5217.390	Fe I	...	6.5
5227.190	Fe I	36.6	...	10.9	...	30.2	31.0	...	35.0	42.5	23.1	15.5
5232.940	Fe I	25.8	...	7.8	...	22.4	20.1	...	28.8	34.7	16.0	8.1
5242.491	Fe I	...	5.6
5250.646	Fe I	...	5.5
5263.305	Fe I	...	6.9
5269.537	Fe I	30.2	...	58.3	66.4	73.9	...	36.4
5328.039	Fe I	23.5	...	51.3	56.8	61.7	...	28.9
5332.900	Fe I
5339.930	Fe I	...	11.5
5341.024	Fe I	11.6	23.4	...	23.1	34.3	...	15.4
5393.167	Fe I	...	10.8
5397.128	Fe I	29.4	...	10.1	...	27.6	24.6	...	31.3	36.4	17.4	10.8
5405.775	Fe I	31.6	...	11.5	...	27.2	27.1	...	32.2	40.6	19.7	13.1
5429.696	Fe I	32.8	...	8.8	...	29.3	28.4	...	35.9	42.4	20.5	12.8
5434.524	Fe I	20.0	...	5.8	33.5	18.5	16.3	...	21.3	26.4	12.0	8.0
5455.609	Fe I	25.4	...	5.9	36.7	22.3	19.2	...	23.8	31.8	13.2	10.1
5497.516	Fe I	...	13.1
5501.465	Fe I	...	10.0
5569.618	Fe I	...	12.1
5572.841	Fe I	10.7	17.8	...	16.0	9.0	6.3	26.6	9.0	14.3
5576.090	Fe I
5586.756	Fe I	14.7	24.4	4.6	23.6	11.3	9.5	33.7	15.7	16.2	9.5	...

Table 6b—Continued

λ (Å)	Ele.	13	14	15	16	17	18	19	20	21	22	23
5658.816	Fe I	...	6.6
4508.289	Fe II	10.5	13.8	3.8	11.7	8.9	5.4	26.3	9.5	14.3	5.8	...
4515.339	Fe II	9.6	9.4	...	9.1	...	3.2	20.3	7.9	10.4	7.0	...
4522.634	Fe II	15.1	15.7	7.1	16.5	9.3	6.2	...	12.2	17.9	9.5	...
4576.339	Fe II	5.0	5.4	10.1
4583.837	Fe II	26.8	28.4	5.8	31.0	18.8	13.0	...	21.0	29.3	16.0	8.5
4629.339	Fe II	9.8	11.7	...	13.6	6.9	4.9	27.0	10.5	12.0	6.1	...
5197.576	Fe II	6.1	6.7	...	10.7	...	5.2	18.2	8.2	9.7	3.5	...
5234.630	Fe II	8.7	8.0	3.5	12.1	22.7	8.4	12.2	5.2	...
5276.002	Fe II	9.2	9.3	...	20.2	...	5.2	28.2	10.6	15.0	6.2	...
4518.023	Ti I	5.3	7.0
4527.305	Ti I	4.9
4533.239	Ti I	4.6	7.0
4534.778	Ti I	11.9	15.3	...	13.9	9.5	7.0	25.9	...	12.4	7.0	5.5
4535.570	Ti I	9.5	6.2	...	5.6	...	3.7	17.2	7.7	6.7	4.1	...
4681.908	Ti I	8.1
4981.732	Ti I	14.2	16.0	4.3	14.0	9.4	8.4	...	10.6	14.5	11.1	...
4991.067	Ti I	11.9	20.9	4.7	19.1	10.5	9.8	24.2	13.3	16.8	...	5.7
4999.504	Ti I	9.9	10.6	...	12.6	...	4.2	21.7	7.7	11.5	4.6	...
5016.162	Ti I	5.3
5020.028	Ti I	5.0
5022.871	Ti I	9.7
5035.907	Ti I	...	5.5	9.2	5.3
5036.468	Ti I	5.0	7.0
5039.959	Ti I	7.9
5064.654	Ti I	8.0
4501.272	Ti II	13.6	...	34.0	24.4	...	38.1	51.5	29.9	13.7
4563.761	Ti II	11.7	...	26.5	19.6	...	30.8	42.7	24.6	13.0
4571.968	Ti II	15.3	...	33.3	24.8	...	36.1	50.6	30.7	13.1
4589.958	Ti II	9.7	11.1	...	9.7	6.1	4.8	27.8	6.2	12.9	4.5	...

